LDEF DATA: COMPARISONS WITH EXISTING MODELS

Cassandra Coombs, Alan Watts, John Wagner and Dale Atkinson
POD Associates, Inc.
2309 Renard Pl, SE
Suite 201
Albuquerque, NM 87106

ABSTRACT

The relationship between the observed cratering impact damage on the Long Duration Exposure Facility (LDEF) versus the existing models for both the natural environment of micrometeoroids[1] and the man-made debris[2] was investigated. Experimental data was provided by several LDEF Principal Investigators, Meteoroid and Debris Special Investigation Group (M&D SIG) members, and by the Kennedy Space Center Analysis Team (KSC A-Team) members. These data were collected from various aluminum materials around the LDEF satellite. A PC (personal computer) computer program, SPENV, was written which incorporates the existing models of the Low Earth Orbit (LEO) environment. This program calculates the expected number of impacts per unit area as functions of altitude, orbital inclination, time in orbit and direction of the spacecraft surface relative to the velocity vector, for both micrometeoroids and man-made debris. Since both particle models are couched in terms of impact fluxes versus impactor particle size, and much of the LDEF data is in the form of crater production rates, scaling laws have been used to relate the two. Also many hydrodynamic impact computer simulations were conducted, using CTH[3], of various impact events, that identified certain modes of response, including simple metallic target cratering, perforations and delamination effects of coatings.

Work performed under contract to Lockheed ESC/NASA Johnson Space Center; Contract No.: 960-12-171, SC 02N0165768. POD Contract No.: 019201

INTRODUCTION

Since the return of LDEF there has been a continuous gleaning of impact data, from both the activities of the M&D SIG and from individual PI's. A large number of impact craters have been studied for almost all possible surface orientations relative to the velocity vector (*i.e.*, the direction of orbital motion, RAM direction), and cover a wide size range from below 10 μm to 5.3 mm. The target materials range from Al 6061-T6 frame components (studied in this report) to various painted surfaces and glasses. The individual craters have been carefully documented with regard to exact position on the various plates, and frame components (longerons and intercostals) of LDEF, and each specific impact event has been studied with regard to crater size, lip dimensions and any associated cracking or delamination (Figures 1a and 1b). The data have been reduced to the form of impact fluences (hits per unit area, or the integral of the crater production rates) versus crater diameter for various surface orientations. These data are then compared with the predictions of the two existing "standard" models for micrometeoroids and debris fluxes for Low Earth Orbit (LEO).

MODELLING THE PARTICLE ENVIRONMENT

POD has written a PC-based computer code SPENV (**SP**ace **ENV**ironment) which incorporates the Cour-Palais[1] model of near-Earth micrometeoroids and the Kessler[2] model of debris in LEO. The code predicts the "impact fluences" (note: we define this term to mean the time-integrated areal density of impacts) as functions of altitude, orbital inclination, specific time period in orbit, and orientation of the LDEF surfaces relative to the velocity vector: *e.g.*, RAM, SPACE, EARTH, SIDES and TRAIL (Figure 2). In the LDEF terminology of some these surfaces are EAST, SPACE, EARTH, NORTH & SOUTH, and WEST, respectively. Since both the micrometeoroid and debris models presently assume symmetry about the velocity vector the two SIDE predictions are normally identical. However, a small misallignment of the RAM surface of 8 degrees introduces a small asymmetry to the data. Details of the SPENV code and its use of the models are given in Atkinson *et al.*[4]

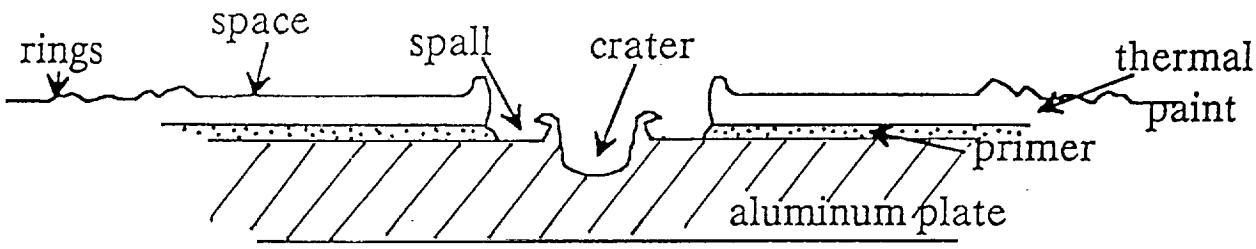

(1a)

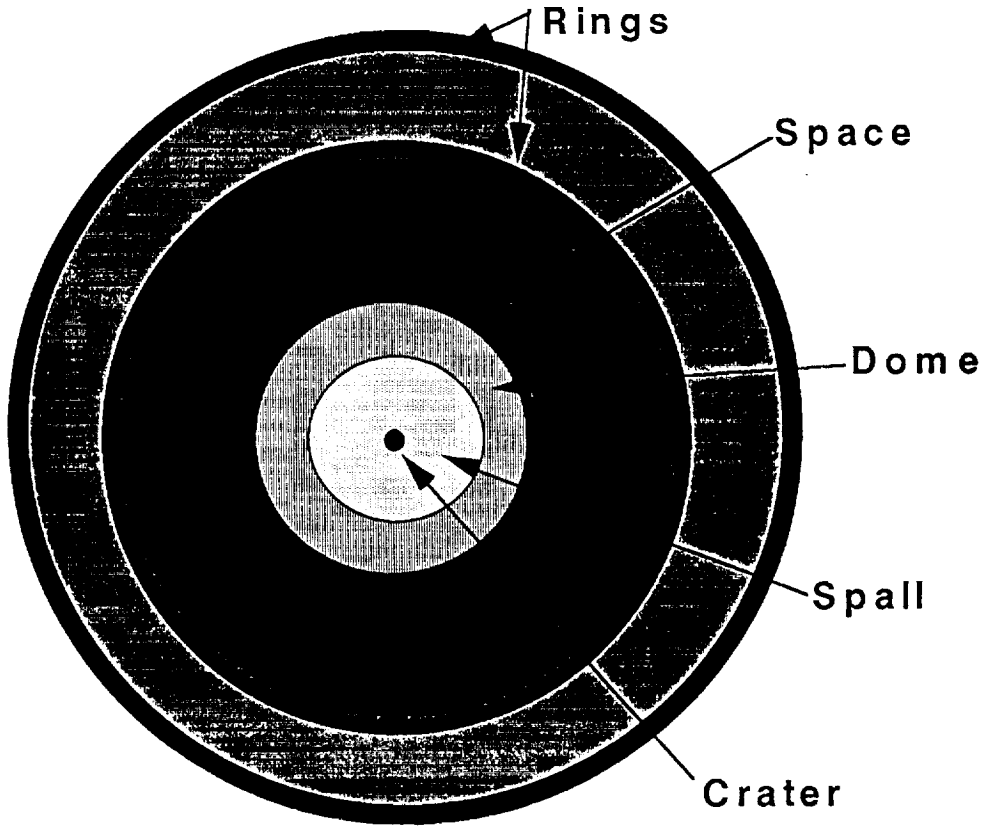

(1b)

Figures 1a and 1b: (a) Schematic cross-section of an impact into painted aluminum. (b) Schematic plan view of a "typical" crater in painted material measured on LDEF. A slight asymmetry is typical for most craters. Note: diagrams are not to scale.

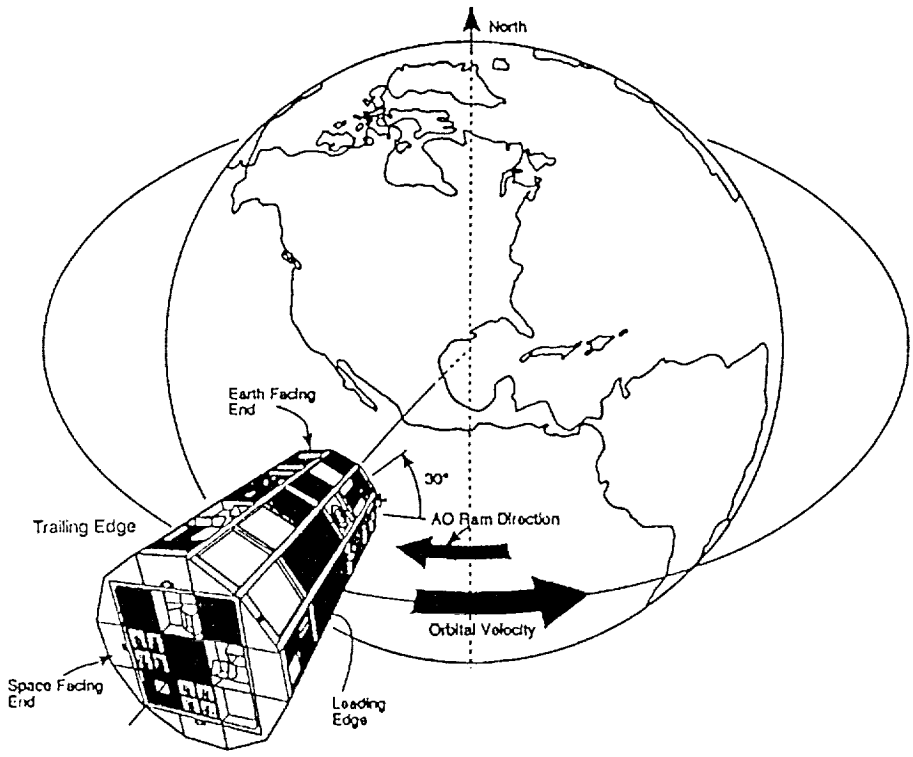

Figure 2: Illustration of LDEF's orientation while in gravity-gradient stabilized Earth orbit. Note RAM, SIDES (top and bottom on figure),TRAIL, EARTH, and SPACE faces.

The micrometeoroid model takes into account the shielding subtended by the Earth as seen by LDEF, and thus is a function of altitude. For cratering predictions the mean density of micrometeoroids has been set at 0.5 gm/cm^3 as suggested by Cour-Palais[1]. (In reality, the true density of micrometeoroids is uncertain. *Captured* particles have had densities of up to 3.5 gm/cm^3. However, the recommended flux model of Cour-Palais is itself based on the lower density and would need revising if the density were changed). The micrometeoroid model assumes that the particles arrive at the Earth uniformly from all directions (*i.e.*, appear geocentric). This is not strictly true, but is a reasonable approximation for the 5.75 year exposure time period of LDEF, since during this time the LDEF orbit underwent about 38 complete cycles of precession and thus "sampled" a large region of the 4π solid angle of space.

The debris model assumes a density of aluminum (2.8 gm/cm^3) for particles about 1 cm diameter, which decreases for larger pieces (since large pieces are not chunky bodies but rather pseudo-porous items such as bits of plates, antennas, and so on), and increases for smaller sizes to about 4.0 gm/cm^3, which is representative of alumina propellent particles and flakes of paint pigment.

The debris model presently assumes pseudo-circular orbits, which immediately prevents collisions on the TRAIL surface of LDEF. The LDEF data, based on impact fluence and both scanning electron microscopy (SEM)[5] and secondary ion mass spectrometry (SIMS)[6] analysis, is revealing that debris particles **did** impact on the TRAIL surfaces. The obvious explanation is that some of the debris are in elliptical orbits. Kessler has been aware of the limitations of his original model, but until recently had little data with which to update it. With the new LDEF data Kessler now concludes that there are significant amounts of debris (*i.e.*, about 20-30 times that tracked by Space Command) in GPS transfer-type orbits at low inclination.[7] This debris should mainly be aluminum oxide effluent from orbital transfer rocket firings.

POD has also independently used an ephemeris code to identify the possible orbit of the particle causing the **largest** crater observed on LDEF. This crater (5.3 mm) occurred on an

aluminum Z-frame on the SPACE end of LDEF, but on a surface facing into the RAM and slightly depressed below the outer envelope of LDEF. In order for the impactor to reach the impact point it must have "come over" the leading edge of the tray, which implies it arrived from the RAM direction but with a SPACE-component angle of at least 15 degrees. The ephemeris code gives a potential solution for a particle in an orbit typical of a GPS transfer stage or for a retrograde launch from Vandenburg. This is in basic agreement with the present conclusions of Kessler.[7] Detailed studies of impacts using the CTH hydrodynamic code (see CTH discussion below) indicate that the most probable source was a piece of aluminum debris. This conclusion is based on determination of perforation limits for either debris or the lower density micrometeoroids.[8] Only a high density particle fits the scenario, ruling out the likelihood of a lower-density micrometeoroid, but allowing the more common high density ones. The inferred particle size is about 1 mm, and for this size the present models predict a higher impact fluence for debris than for micrometeoroids, again suggesting that the impactor was debris. Recent chemical analysis of this impact feature (M. Zolensky, private communication) reveals the presence of no non-Al material (a *null* result) which is still consistent with almost any kind of impactor.

MODEL SCALING LAWS

Whereas the environment models are given in terms of particle diameters, all of the data from LDEF is in the form of impact feature diameters. In order to relate the two for craters it is necessary to invoke a scaling law to give crater sizes versus impactor sizes. The SPENV code presently invokes the simplest of the known cratering laws, namely the "energy" law. This law equates the incoming kinetic energy of the impactor with the energy necessary to "carve out" a hemispherical crater. The result is:

$$D_c/D_p = \text{constant } (\rho_p/\rho_J)^{0.333}\, u^{0.666} \qquad (1)$$

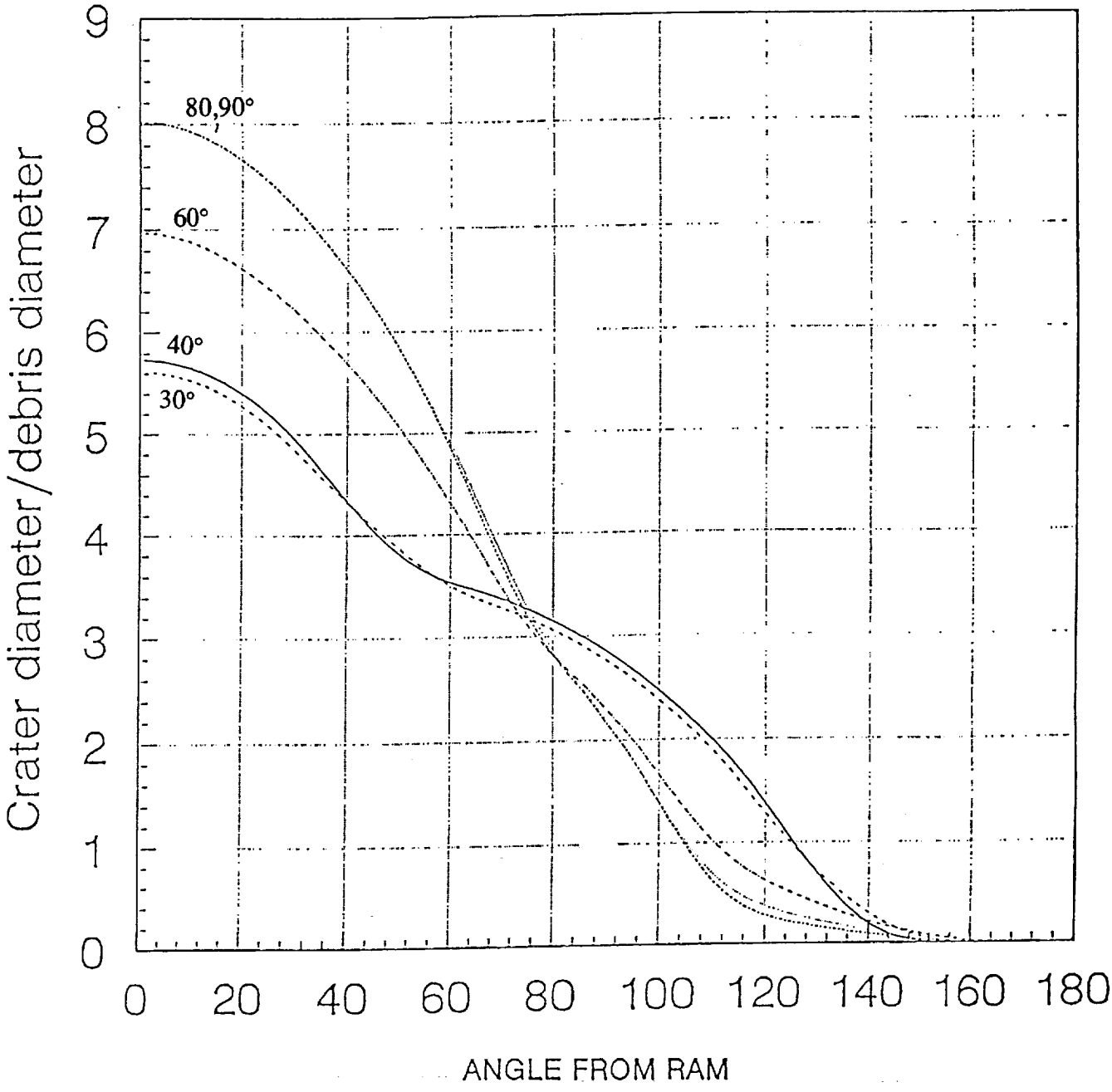

Figure 3: Plot of Dc/Dp versus angle from RAM for debris, in the plane parallel to the Earth. The numbers adjacent to the curves indicate the orbital inclination for that particular curve.

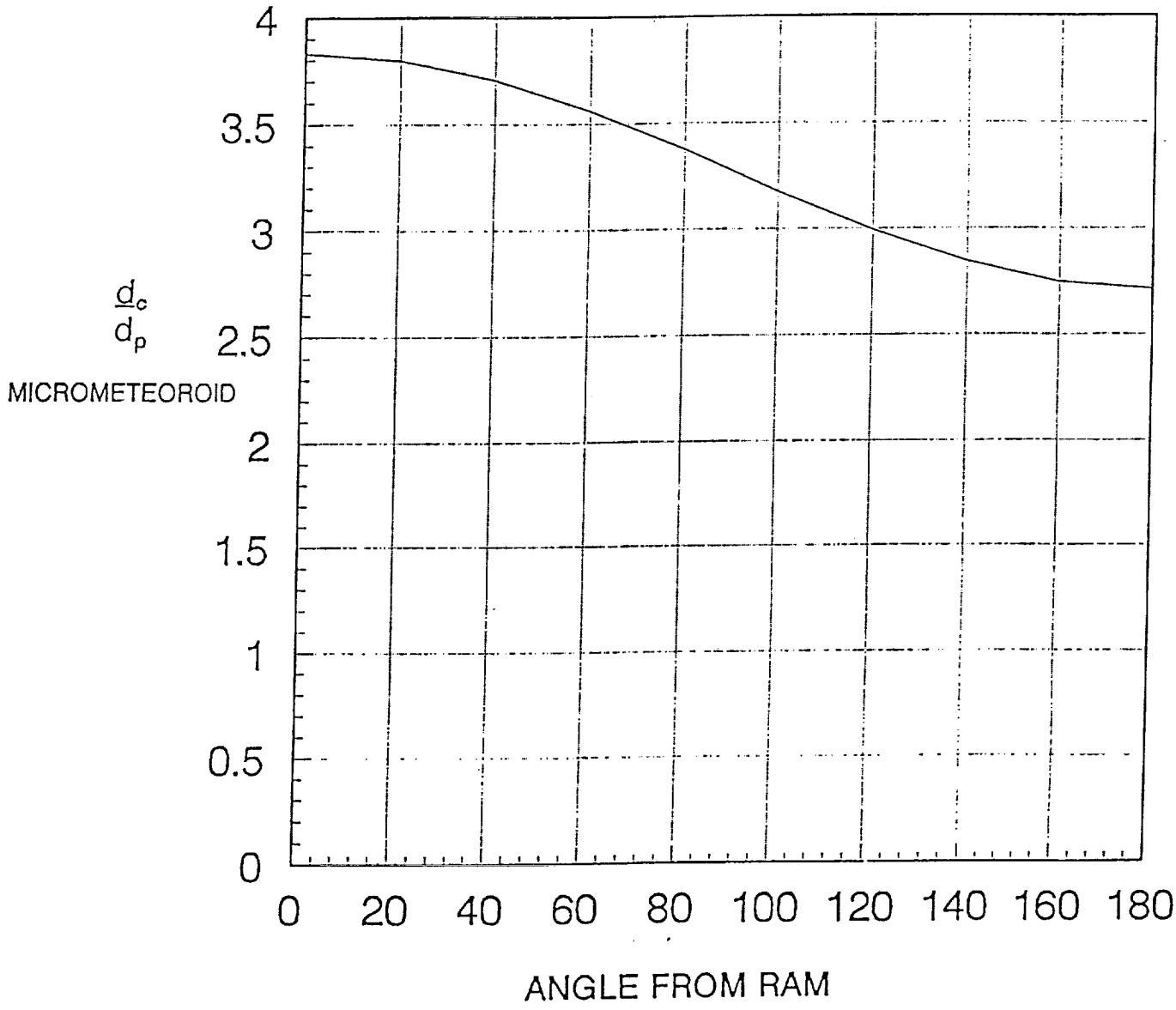

Figure 4: Plot of Dc/Dp versus angle from RAM (velocity vector) for micrometeoroids, assuming a density of 0.5 gm/cm^3, in the plane parallel to the Earth.

where D_c is the crater diameter, D_p is the particle diameter, ρ_p and ρ_t are the impactor and target densities, u is the impactor speed normal to the target surface, and the constant is determined by laboratory experiments.[8] This equation is sensitive to the normal component of impact velocity, and the existing particulate models predict that practically **none** of the impacts are normal. Further, the impact velocities are themselves functions of arrival direction and thus of the orientation of a specific surface relative to the RAM. Consequently, the value of D_c/D_p is a function of surface orientation which is also a function of orbital inclination, and, in principle, of altitude. Figures 3 and 4 illustrate this dependence for debris and micrometeoroids, respectively.

Figure 5 shows the distribution of relative debris impacts in the form of a polar plot versus the RAM direction ("butterfly plot") based on the Kessler model. These impacts are in the plane parallel to the surface of the Earth. The corresponding impact speeds are given by the relation $v = 15.4 \cos A$ km/s, where A is the angle between the RAM direction (zero degrees) and the apparent approach direction of the debris. The component of the impact velocity along the normal to a surface is given by $v = 15.4 \cos A \cos (B-A)$ km/s, where B is the angle between the surface normal and the RAM direction. For the RAM surface itself this reduces to the value $v = 15.4 \cos^2 A$ km/s. If the angle (B-A) exceeds 180^0 then impacts cannot occur on that surface. The data in Figure 3 is obtained by integrating over all the possible angles of approach for a specified surface, based on the relative weighting given by the Kessler model (this weighting explains the butterfly shape).

Figure 6 shows the distribution of **average** impact speeds versus approach direction for the micrometeoroids (RAM direction equals zero degrees). This polar plot represents a body of revolution symmetric about the RAM axis. The effect of Earth-shielding is to remove a section of the solid angle for this figure, which results in a modification of the impact fluxes for all surfaces except that facing towards SPACE. The source of data for this plot is that due to Erickson[9] which describes the relative number of micrometeoroids versus speed as seen from the Earth (so-called "stationary satellite" data). This data is transformed into the reference

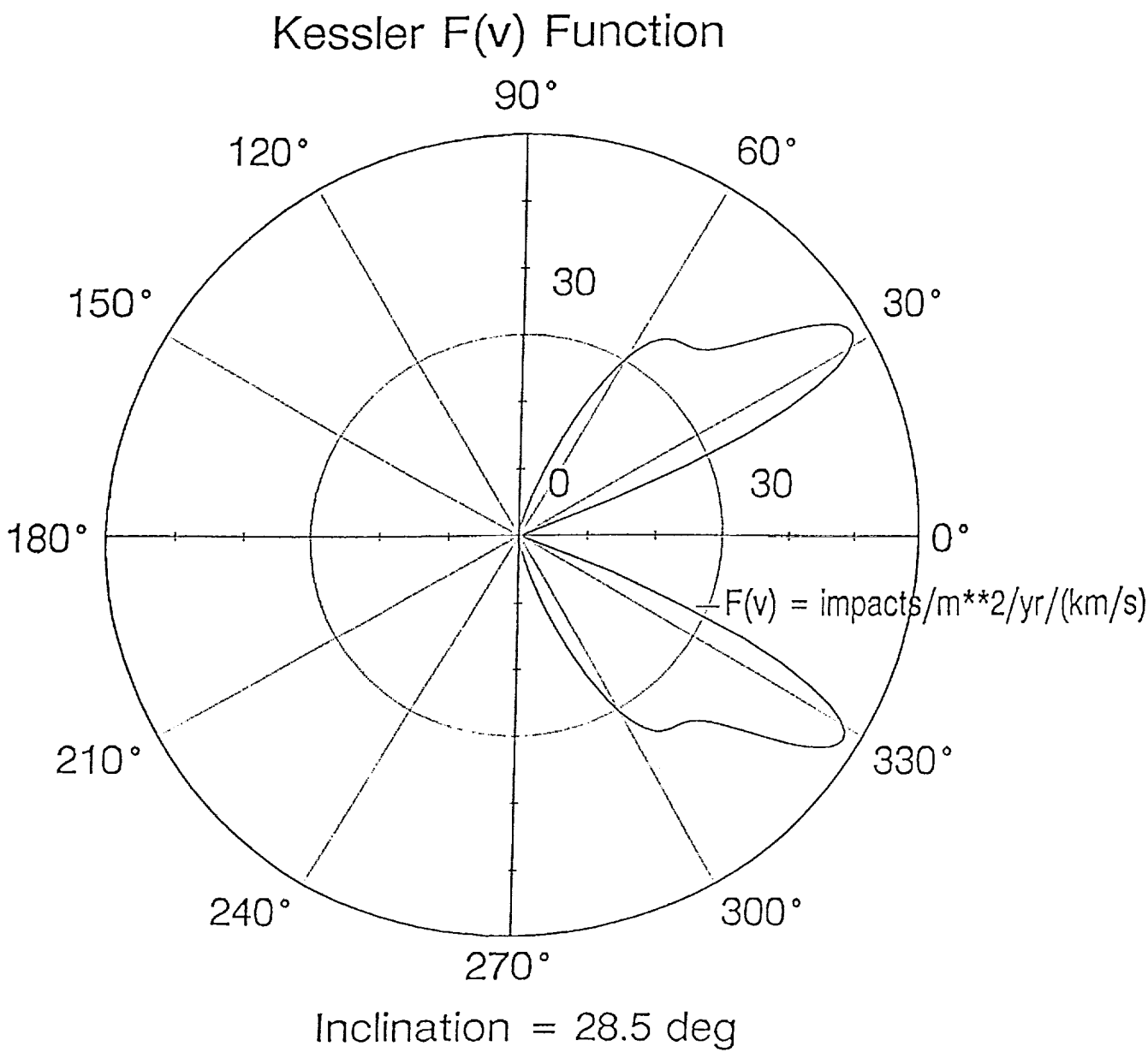

Figure 5: Plot of polar distribution versus angle from RAM (velocity vector) for debris, in the plane parallel to the Earth, for LDEF.

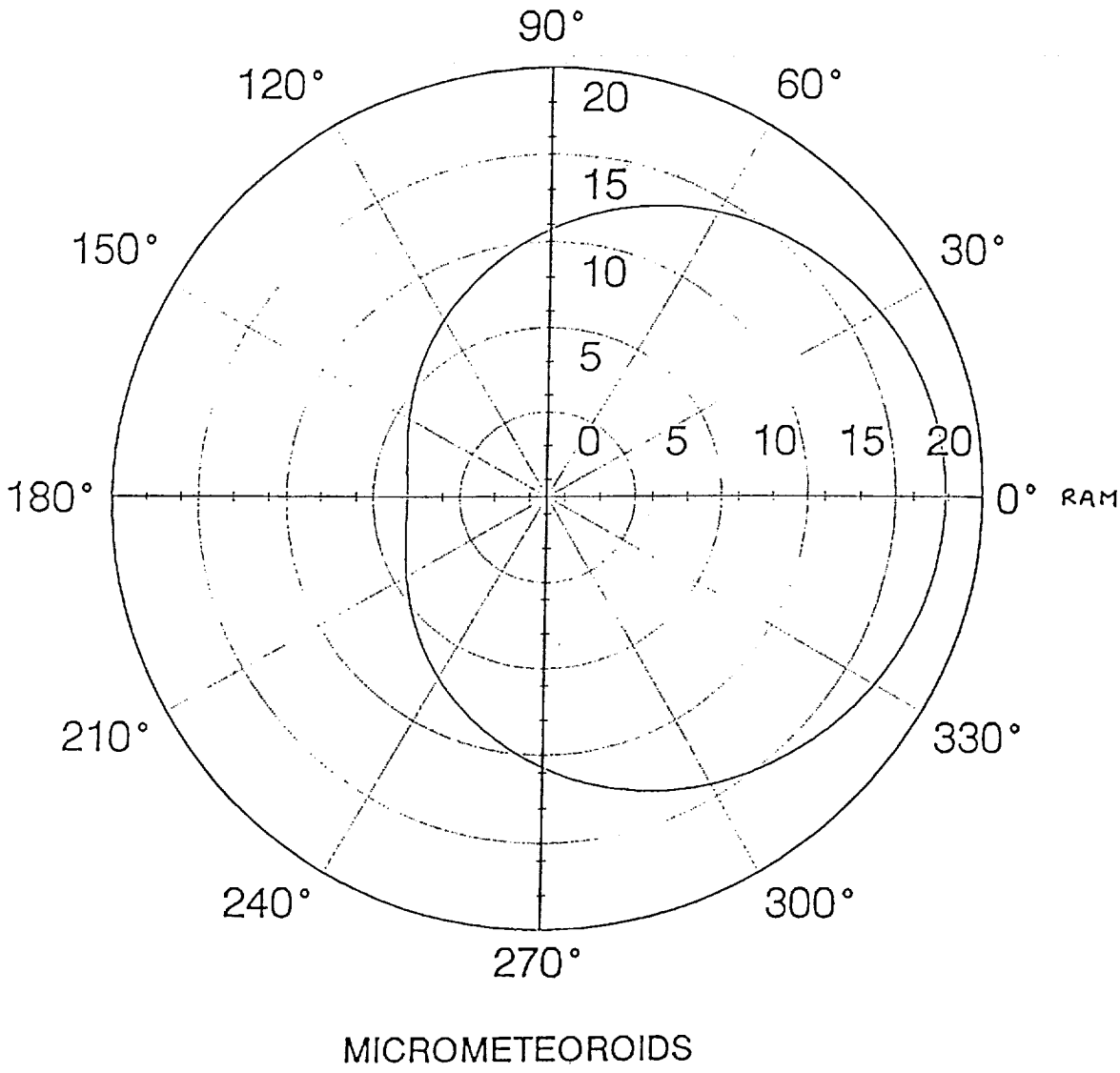

Figure 6: Plot of polar distribution of impact velocity versus angle from RAM (velocity vector) for micrometeoroids. This figure is axisymmetric about the RAM axis, and ignores Earth shielding.

frame of the orbiting satellite to produce Figure 6. As with debris the effects of micrometeoroid impacts are obtained by integrating over all particles taking into account the components of velocity along the normal to the specific surface.

There are several other proposed crater scaling laws (*e.g.*, Cour-Palais[1,10] and Christiansen[11]). In general, the differences in these laws are variations in the power indices for densities (and/or masses) and velocity. Since the indices are less than unity, the effect is a relatively small shift in the values of D_c/D_p. The data are presented in the form of cumulative fluences, or rather, impacts per area for craters greater than or equal to a specified size, versus crater size. The effect of changes in scaling law is primarily a horizontal shift in the plots. For example, changing the power index for density from 0.333 to 0.5 moves the curves by only a factor of 1.34 even for the extreme case of a tantalum impactor (density 16.6 gm/cm^3) into aluminum (density 2.8 gm/cm^3), and clearly has no effect for symmetric impacts such as aluminum into aluminum. Likewise, a change in the assumed density of a micrometeoroid (*e.g.*, from 0.5 gm/cm^3 to 3.0 gm/cm^3) produces a factor of 1.82 or 2.45 for power indices of 0.333 and 0.5, respectively.

CTH HYDROCODE CALCULATIONS

The CTH computer code[3] from Sandia Laboratory, Albuquerque, has been used to simulate several classes of impacts. In order to benchmark the code, specific calculations were done to replicate laboratory-generated ballistic penetration (*i.e.*, perforation) cases for aluminum. These data were provided by Fred Hörz of NASA JSC. Material parameters were adjusted in the CTH runs until good replications were obtained. The agreements involved standard, acceptable Equation of State (EOS) and constitutive data for the impactors and targets, and in particular, identified the aluminum targets as Al 1100 with temper H16 (Hörz could not specify the exact temper of his samples, but the suggested solution is very credible being a reasonably common alloy). Details of these comparisons are given in the Appendix.

The CTH results were then plotted as functions of perforation limits for various aluminum sphere diameters versus normal impact velocities, and for various aluminum wall thicknesses, and the data were fitted analytically by least-squares techniques. The result was a fit very similar to the perforation-limit conditions predicted by the McDonnell equation.[12] Within the accuracy of determination of the "best-fit" equation for the CTH data, the results essentially agreed with the predictions of McDonnell, except for about a 20% decrease in the prediction of wall thickness. Based **only** on this fact, we presently recommend use of the McDonnell equation for perforation predictions, at least for symmetric Al/Al conditions (*Note*, we have **not** yet validated the "strength" term in the McDonnell equation). This equation is:

$$T = 1.023\ d_p^{1.056}\ (\rho_p/\rho_t)^{0.476}\ (\sigma_{Al}/\sigma_t)^{0.134}\ u^{0.664} \qquad (2)$$

where T is the wall thickness, d_p is the particle diameter, densities (ρ) refer to particle or target, respectively, σ values are the yield strengths of Al or the target, and u is the normal impact speed. For a symmetric aluminum into aluminum (Al/Al) impact this becomes:

$$T = 1.023\ d_p^{1.056}\ u^{0.664} \qquad (3)$$

The corresponding "best-fit" from CTH for Al/Al impacts was:

$$T = 0.81\ (+/-\ 0.20)\ d_p^{0.9375\ (+/-0.105)}\ u^{0.625\ (+/-0.09)}\ \text{(ref.8)} \qquad (4)$$

CTH has been used to simulate impacts on coated materials in order to understand such effects as the "ring" and "dome" structures seen on painted aluminum, together with localized delamination effects. To date, the CTH runs have been able to simulate the formation of "domes" and demonstrate the development of delaminations. However, while the runs have predicted transient "ring" motions (*i.e.*, Rayleigh wave ripples propagating away from the impact site), we have not yet identified the parameters necessary to cause a "freezing" of these waves to yield permanent rings. It appears that the behavior is very sensitive to the amplitude

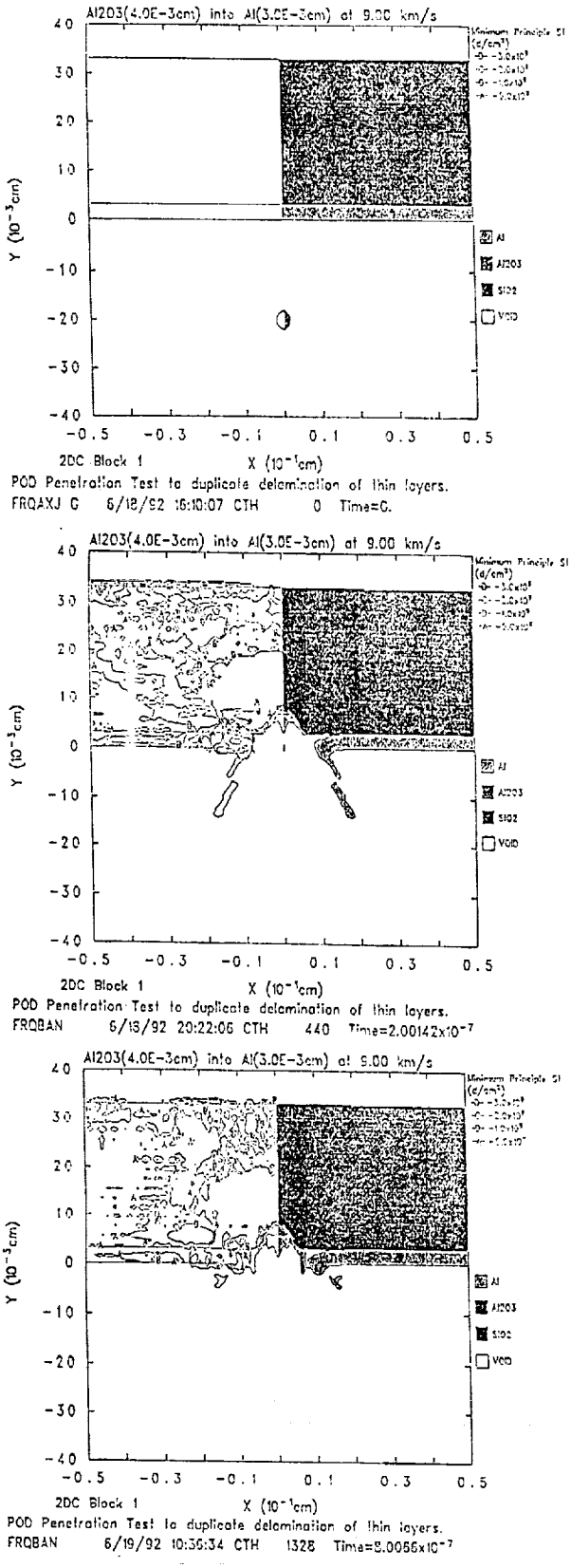

Figure 7: Example results from a CTH run where an alumina projectile impacted a 2-layer target at 9.0 km/s. Time is in sec. Note the factor of 100 vertical exaggeration.

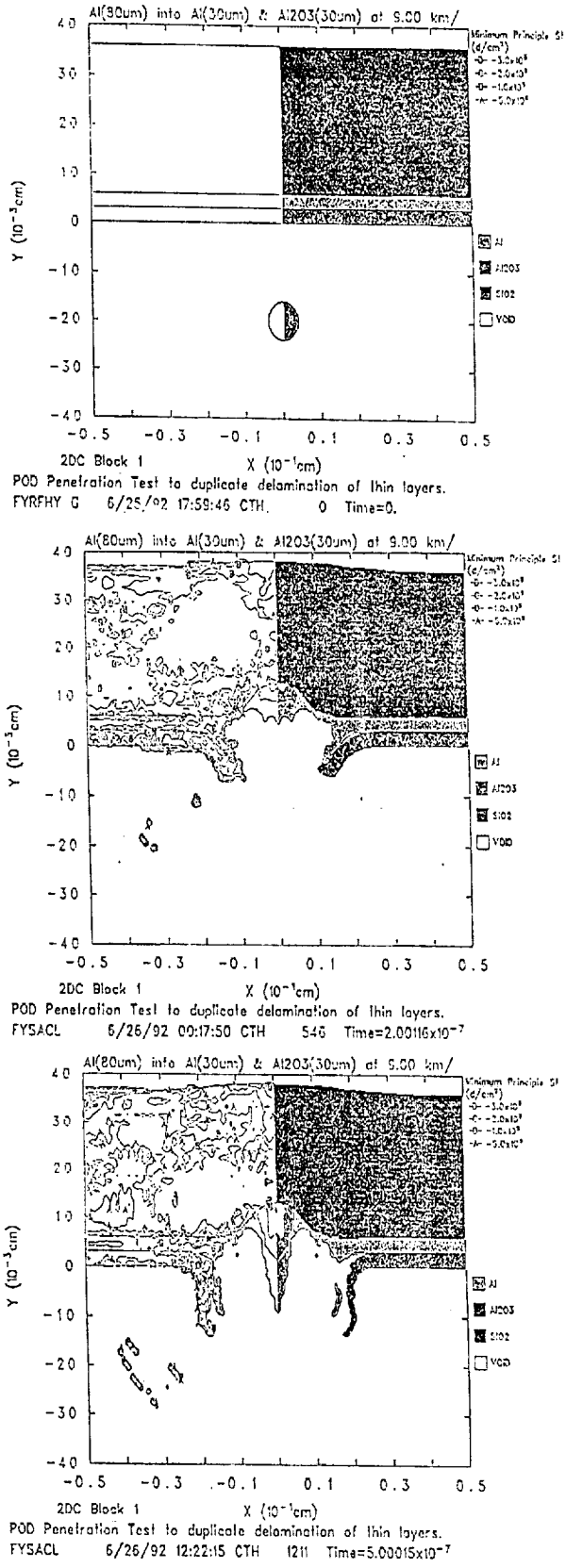

Figure 8: Example results from a CTH run where an aluminum projectile impacted a 3-layer target at 9.0 km/s. The bottom figure shows the impactor jetting back out of the crater.

of the induced wave structure and the yield strength of the materials, since the CTH calculations either gave rapidly dampened waves or else indicated material loss due to localized jetting around the impact site. We do **not** presently understand this since basically **all** of the painted surfaces exhibited "rings" and the impact conditions cannot have been identical. Figures 7 and 8 show some typical CTH results. These example problems include an aluminum coating on a silica substrate (Figure 7) and a two-layer alumina/aluminum coating on silica (Figure 8). In both cases the impactors have been alumina or aluminum. Parameter options investigated include impact speed and interlayer adhesion strength. In each figure, the sequence progresses from the top to bottom, with the top image at 0 time. Projectile velocity was 9.0 km/s for both examples.

The effect of interlayer (bond) strength is interesting. For zero strength the layer locally "peels back" by a small amount around the impact hole in the layer and the layer debonds rapidly in a radial manner away from the hole, such that the entire layer essentially jumps off the substrate. The silica substrate develops a typical crater. As the bond strength is increased so the debonding becomes limited to a region around the impact site, but at the expense of greater localized peel back at the hole edge. Depending on details, the local peel back can resemble the standard lips for a metal target impact, or can spall off and cause secondary ejecta. If the coating is a brittle one (alumina) with high compressive yield strength but low fracture strength, the tendency is to crack off the lips. Conversely, for the soft metal (Al) coating the tendency is to develop considerable plastic/molten flow, and droplets peel off.

In all high speed (>9 km/s) impacts modelled to date, the impacting particle (whether brittle alumina or soft aluminum) has always been forged into a self-forming jet structure which expels itself back out of the hole. This occurs because the impact pressures are sufficiently high to cause gross plastic flow at elevated (shock induced) temperatures, and the geometry causes convergence effects, thus producing the jet. The result is that only small portions of the impactor remain within the crater. We cannot presently identify the exact amount of material remaining, since this involves "late-time behavior" and requires long computer run times. This

behavior is consistent with many LDEF observations, where frequently the impactor is either difficult or impossible to identify due to limited or zero remnants. In particular, the calculations indicate that the impactor does **not** need to completely vaporize in order to explain negligible remnants. For the two-layer coating problem both layers peel back and delaminate from each other and the substrate. Figure 8 shows such a case, and indicates the complicated morphology around the impact site.

Of relevant interest to this discussion is some data provided by Maxwell Laboratory, San Diego.[13] Workers there used the flash X-ray machine, *Blackjack 5*, to throw debris particles at single crystal silicon. The latter target was simultaneously surface heated by the associated X-ray plasma. The result was the development of ring structures very similar to those seen on LDEF. The pictures resemble a frozen version of the "stone in a pond" effect! The postulated explanation is that the hot surface (almost molten) of the silicon was forced to undergo plastic yielding due to the Rayleigh waves, and that hysteresis "locked in" the ripples.

LDEF EXPERIMENTAL RESULTS

Data utilized in this portion of the study originated from three sources: (1) For craters larger than 0.05 cm diameter, measurements were taken by the LDEF Meteoroid and Debris Special Investigation Group's (M&D SIG) Kennedy Space Center Analysis Team on the entire LDEF aluminum structure,[14] and (2) for craters larger than 0.01 cm diameter, measurements were taken by the authors from specific aluminum experiment tray covers and sun shields, and (3) for craters larger than 0.001 cm diameter, measurements were taken by See *et al.*[15] on LDEF intercostals. Separate environment models were utilized to make predictions for the meteoroids and debris and computed using the SPENV model. For meteoroids, the Cour-Palais *et al.*[1] model was used with the Kessler-Erickson velocity distribution as described by Zook.[9] For debris, the Kessler model[2] was used. Our SPENV program models both the micrometeoroid and debris environments that may be encountered by a spacecraft in an orbit

between 200 and 2000 km. As both the Kessler and Cour-Palais models[1,2] predict particle diameters, the scaling law presented previously was applied to these data, thus reducing them to the form of cumulative impact fluences (hits per square meter) for craters greater than or equal to specified diameters.

LDEF was a gravity-gradient stabilized satellite, intended to always have one surface facing EARTH, and one side (row 9) always facing into the RAM. In actuality, LDEF was slightly rotated about its long axis such that row 9 was about 8 degrees off of the true RAM (towards the SOUTH). This fact explains the angular quotes for the intercostals and rows, given below.

Figures 9a-l and 10a-e illustrate the data, together with comparisons of the existing micrometeoroid and debris model predictions. Each of the plots in Figure 9 compares measured crater diameters to the number of craters per square meter (fluence) for different locations on LDEF: RAM (row 9, 352 degrees) through 22 degrees (row 10) (anticlockwise, as viewed from the Earth). For directional reference and location purposes, the plots refer to various intercostals (aluminum frame pieces which run "around" the LDEF central axis), and the corresponding rows (*i.e.*, faces), from LDEF. Each plot shows the data collected from the intercostal and other components in that same row as compared to the meteoroid and debris models. For example, data for craters larger than (say) 500 μm originated from the intercostal which was scanned for that row, and the fluence was derived by dividing by the area of the specific intercostal. A similar process was done for all craters larger than 500 μm on other surfaces as well. Figures 10a-e illustrate the comparison between the LDEF data to the M&D model predictions as a function of row or intercostal location on the satellite (degrees from RAM) vs. fluence. These plots represent the number of craters with diameters greater than or equal to 50 μm, 100 μm, 250 μm, and 500 μm, respectively. **In general**, the sum of the model predictions agrees within a factor of two to three for surfaces toward the RAM. However, toward the TRAIL the agreement is worse by a factor of four or more.

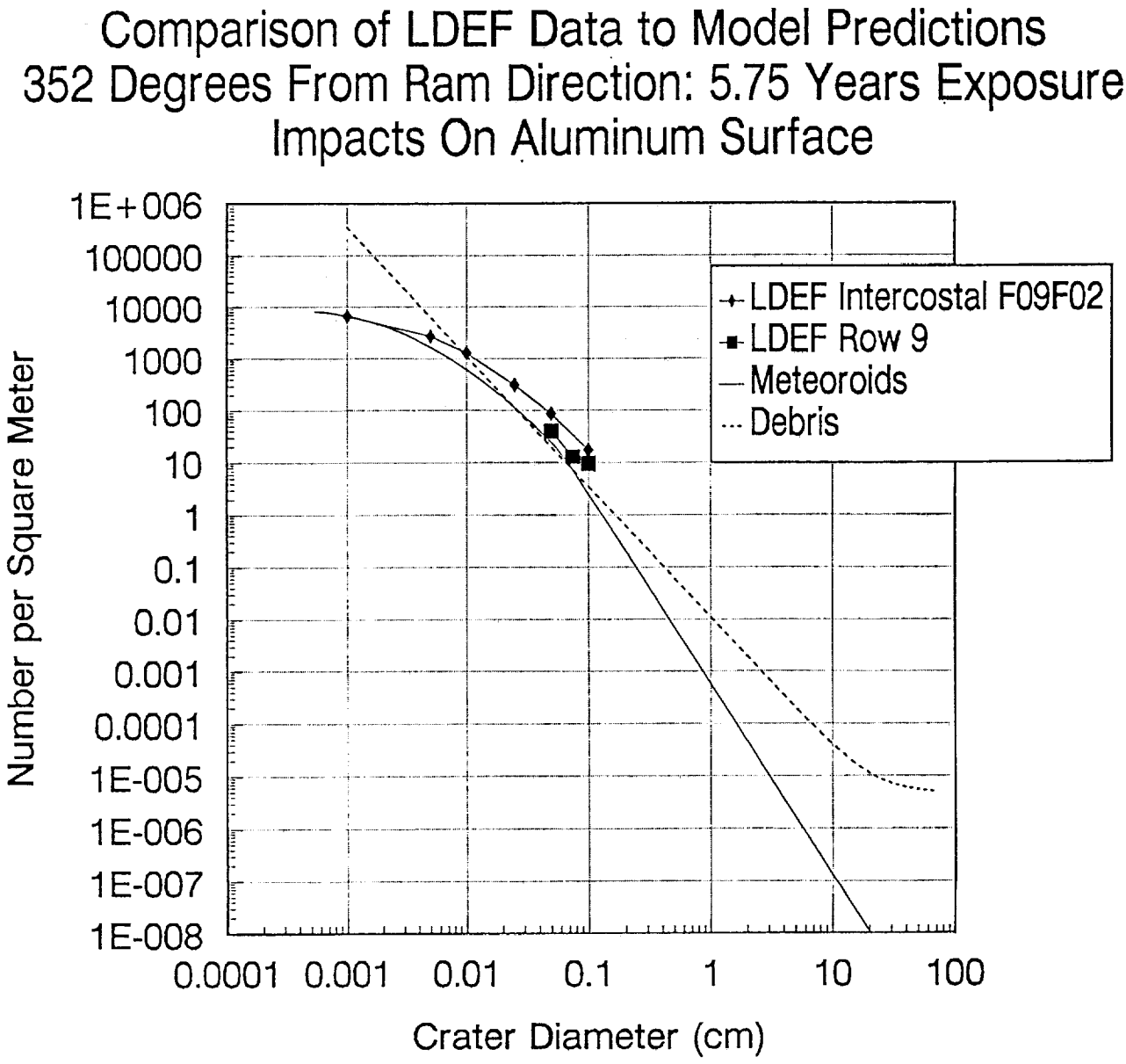

Figures 9a: Comparison of crater diameters to number of craters per square meter. Data collected from the LDEF intercostals and rows.

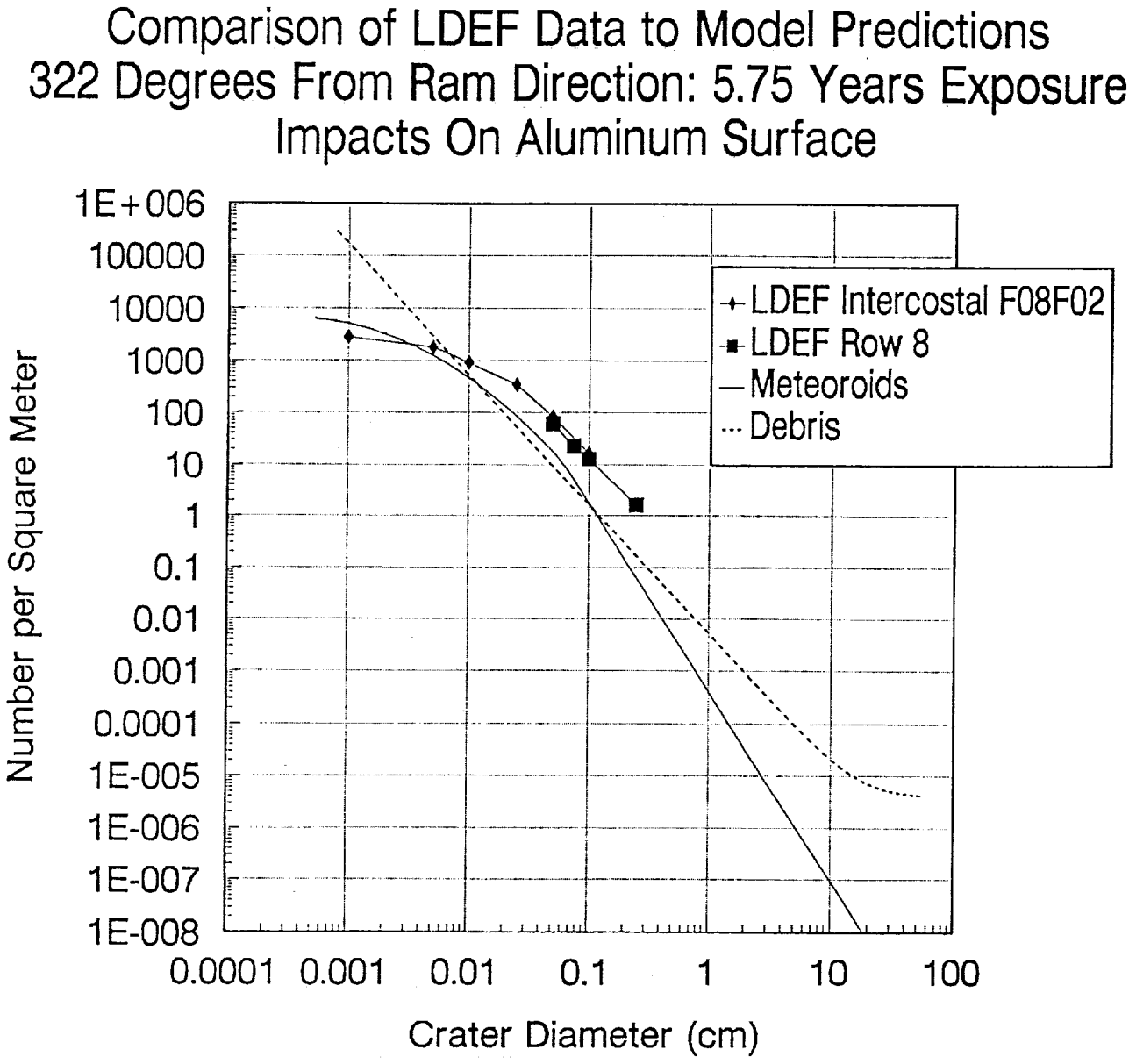

Figures 9b: Comparison of crater diameters to number of craters per square meter. Data collected from the LDEF intercostals and rows.

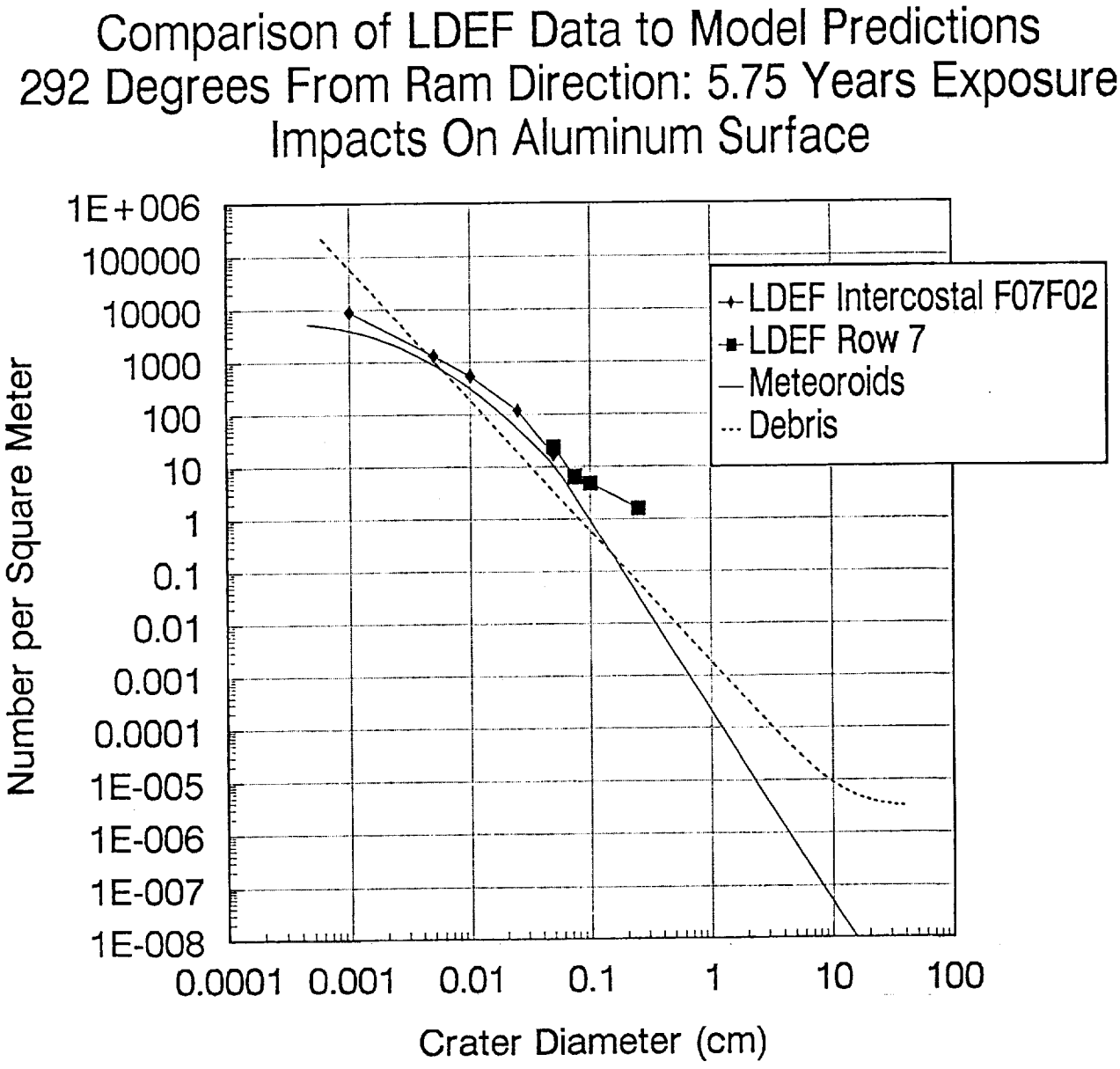

Figures 9c: Comparison of crater diameters to number of craters per square meter. Data collected from the LDEF intercostals and rows.

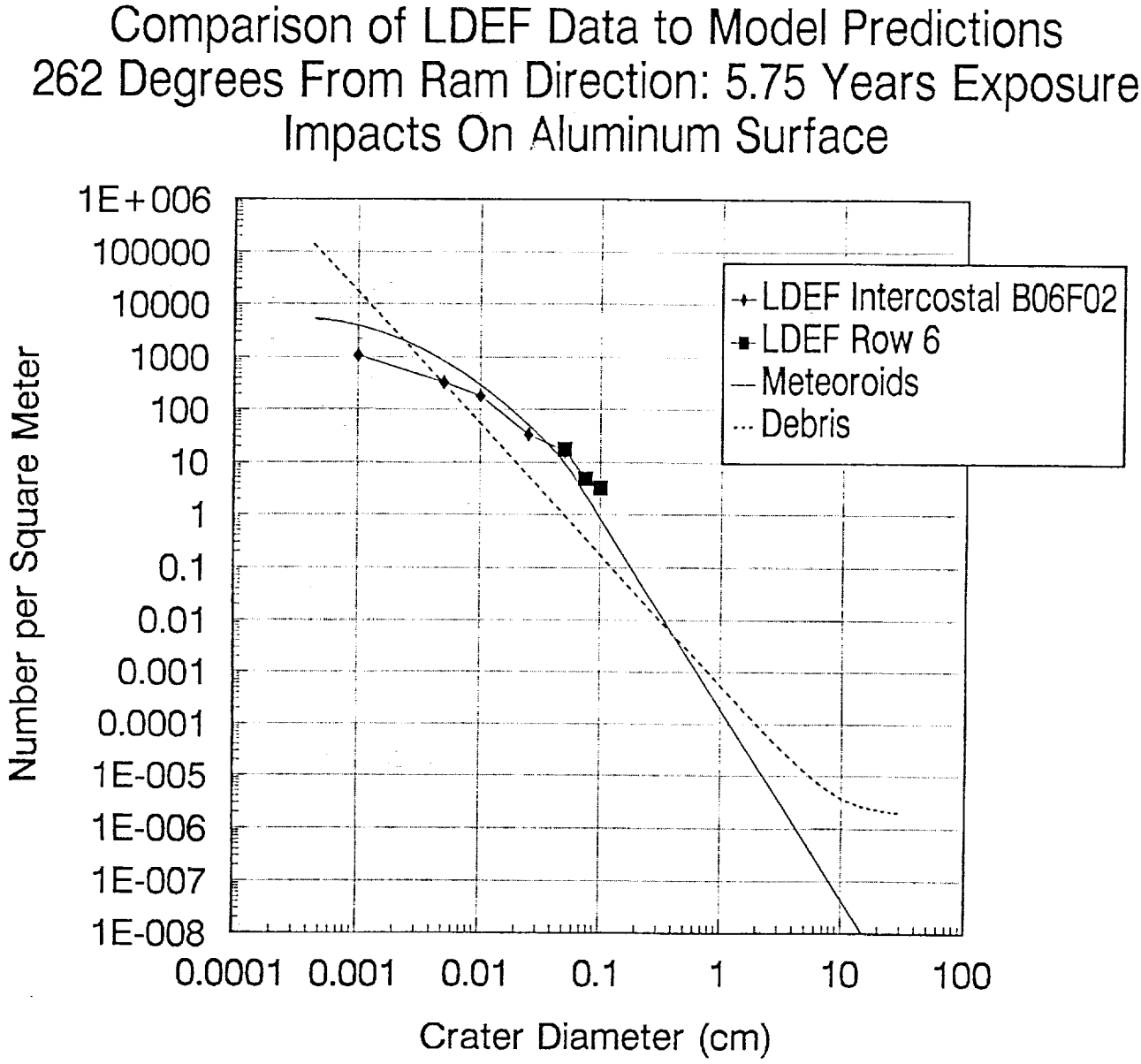

Figures 9d: Comparison of crater diameters to number of craters per square meter. Data collected from the LDEF intercostals and rows.

C-5

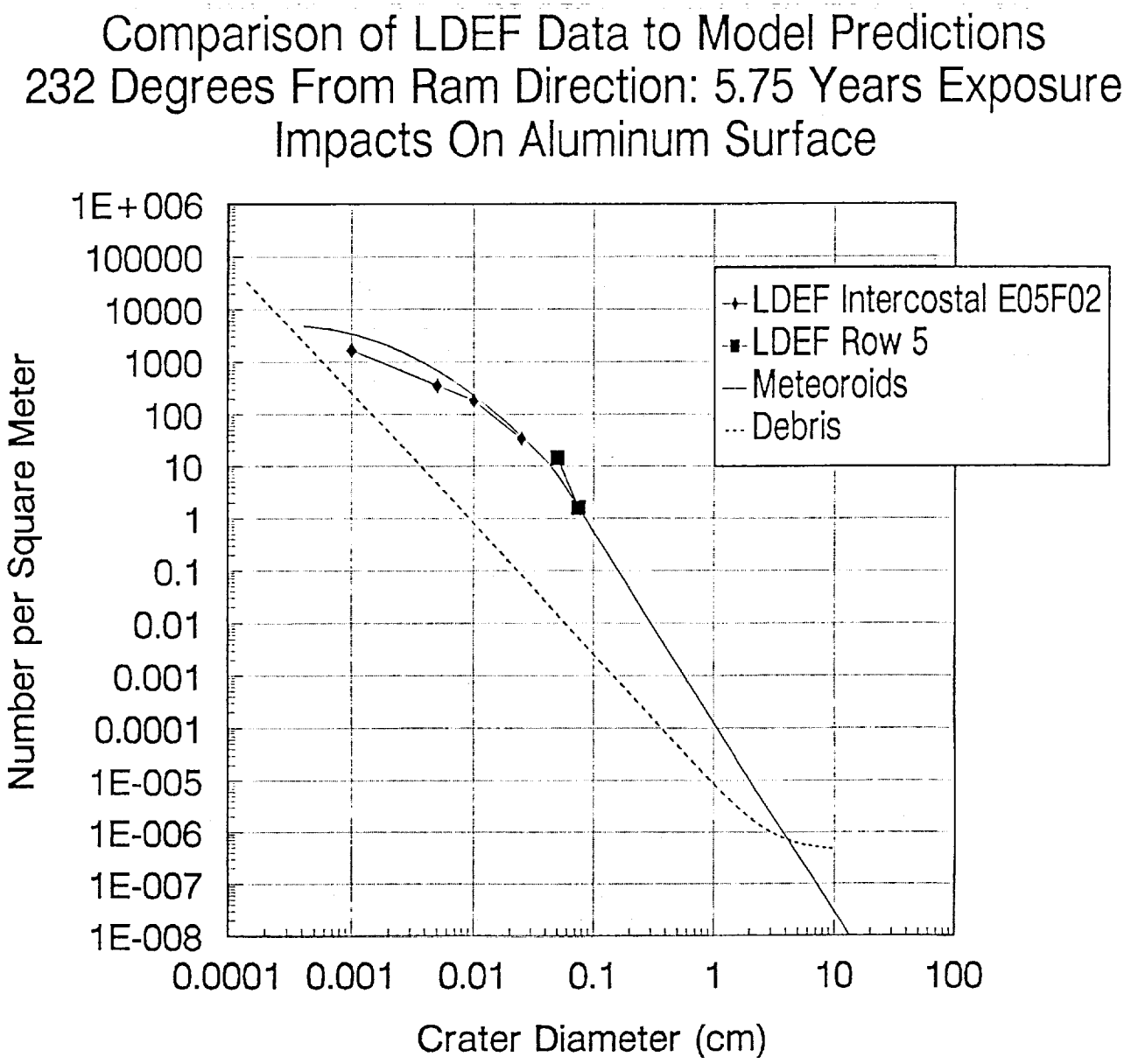

Figures 9e: Comparison of crater diameters to number of craters per square meter. Data collected from the LDEF intercostals and rows.

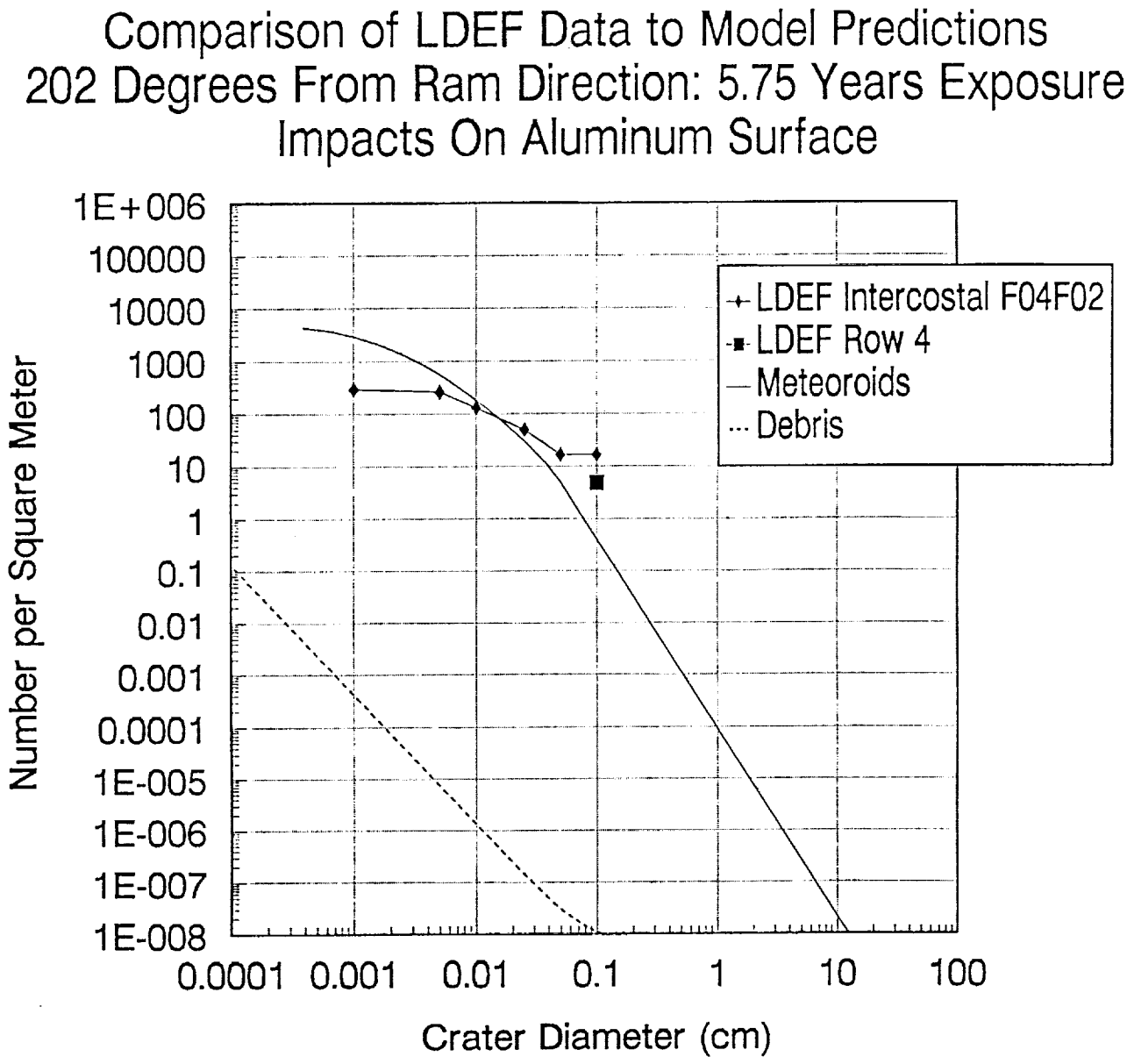

Figure 9f: Comparison of crater diameters to number of craters per square meter. Data collected from the LDEF intercostals and rows.

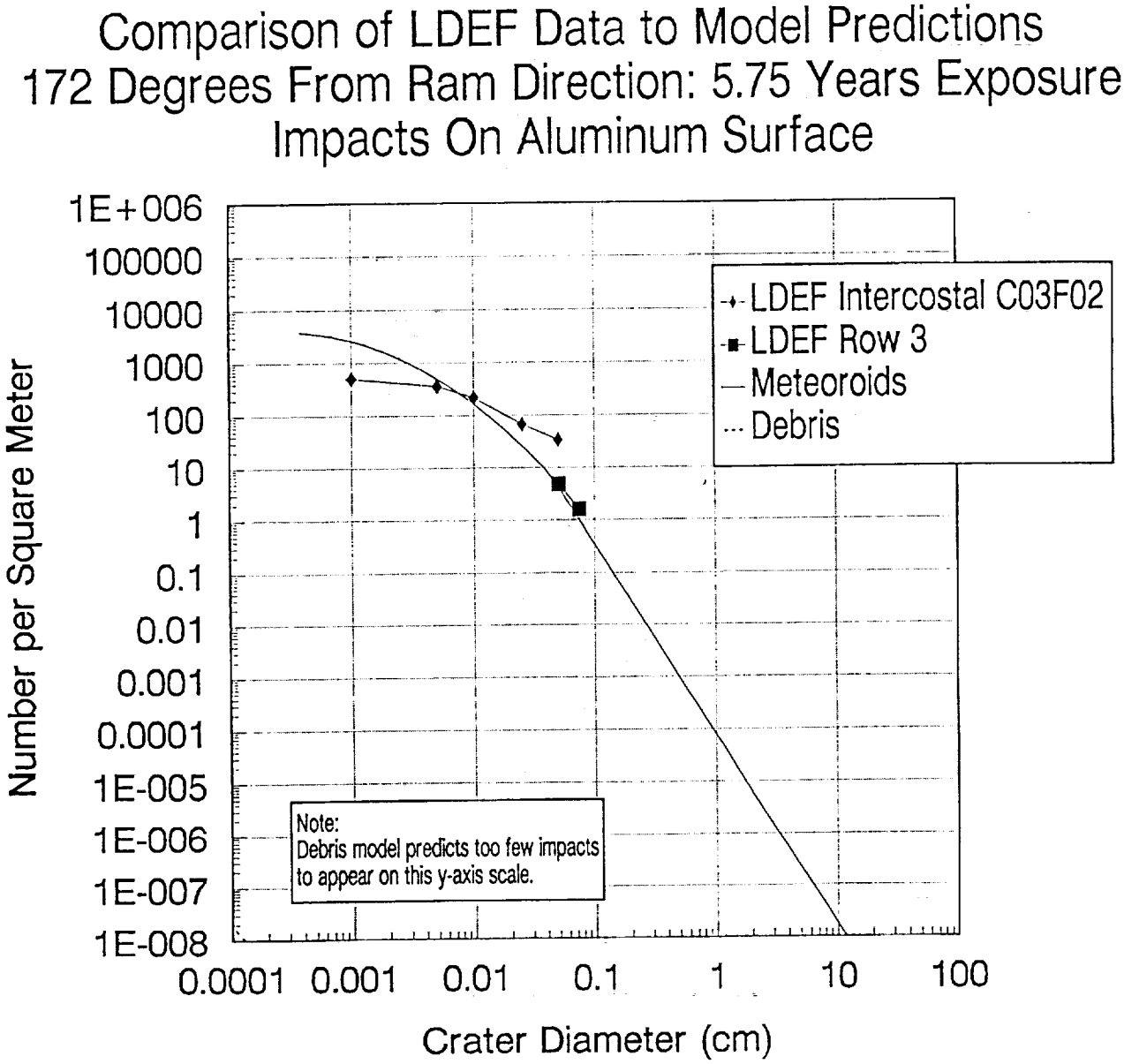

Figures 9g: Comparison of crater diameters to number of craters per square meter. Data collected from the LDEF intercostals and rows.

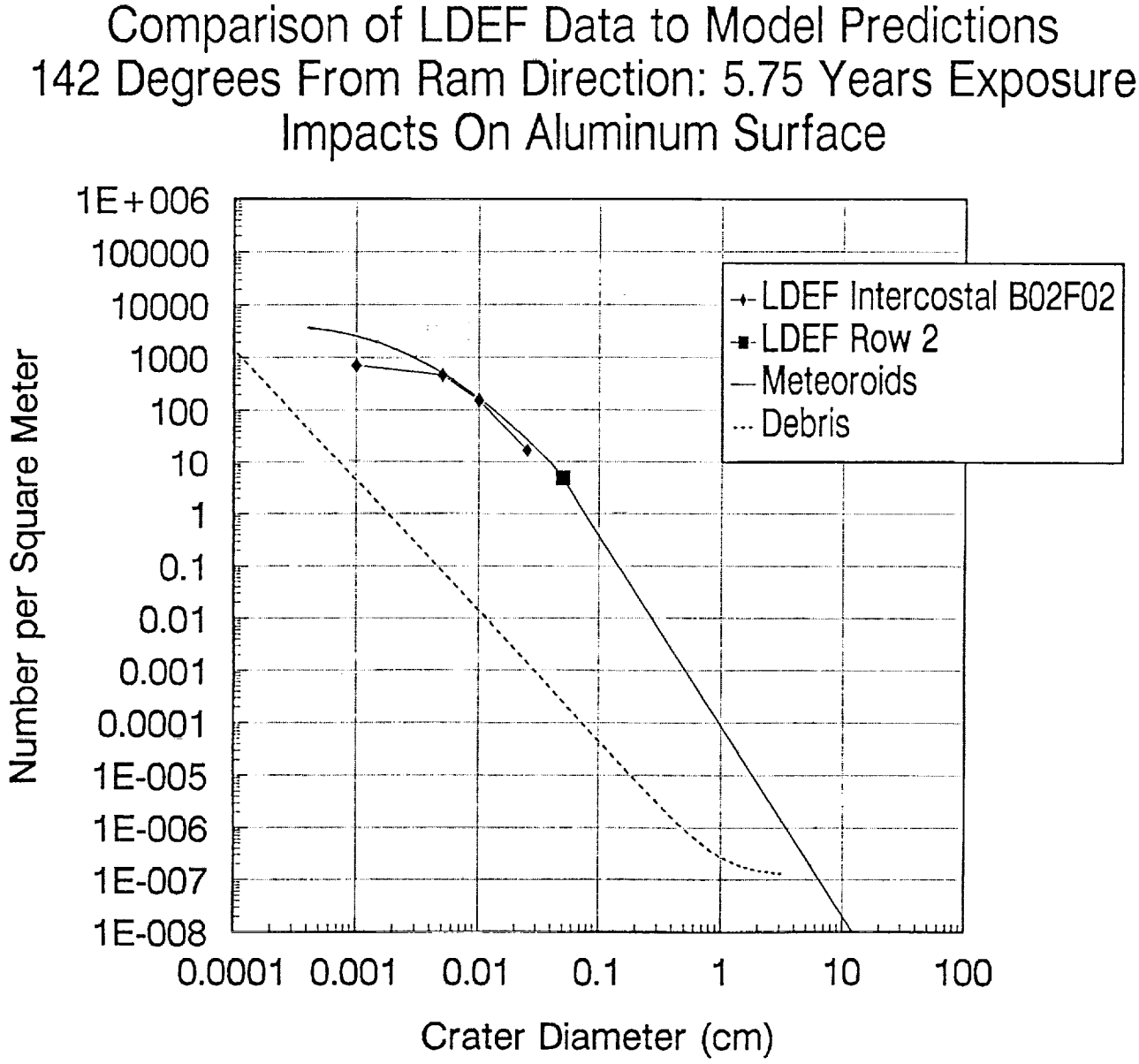

Figures 9h: Comparison of crater diameters to number of craters per square meter. Data collected from the LDEF intercostals and rows.

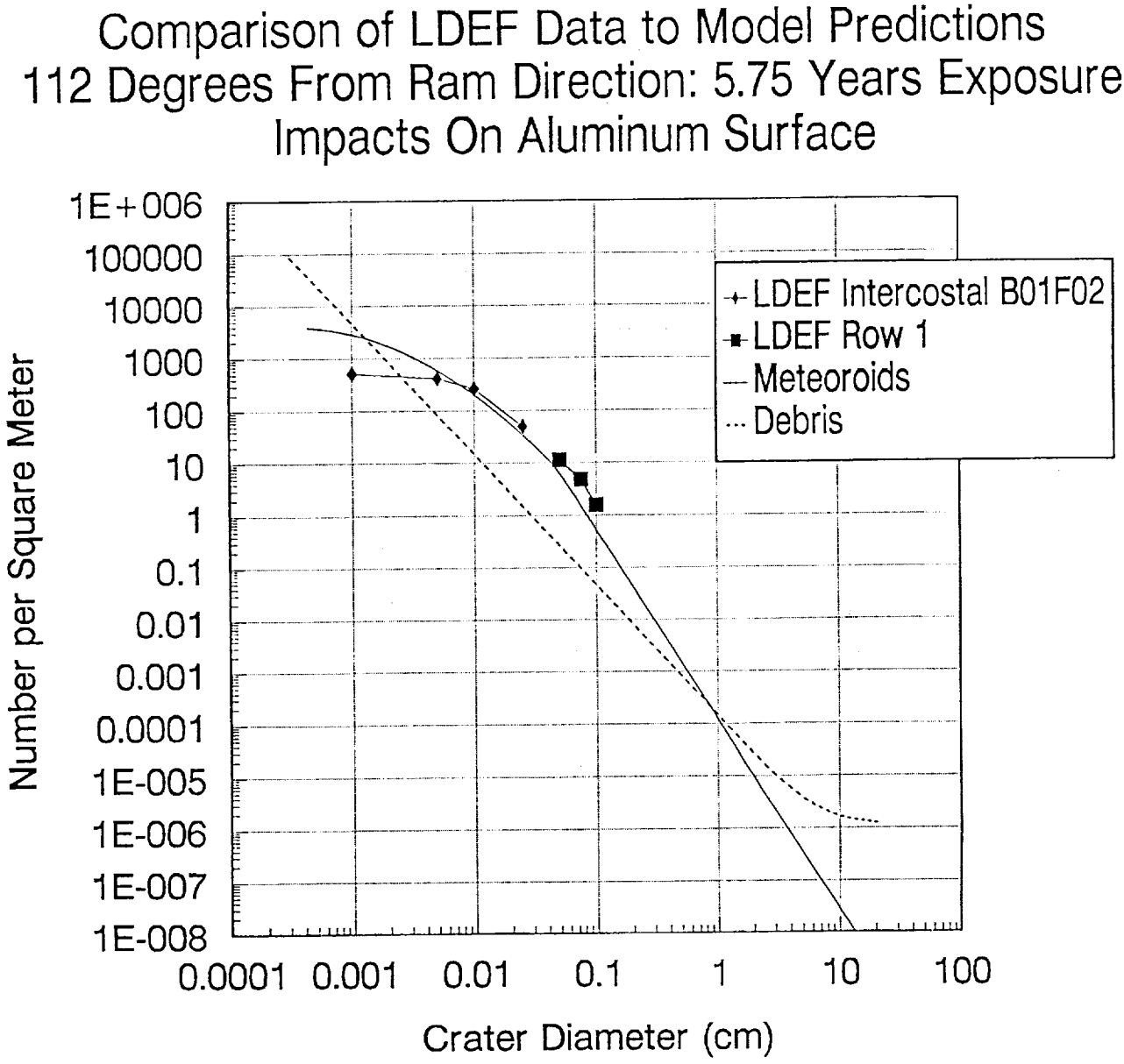

Figures 9i: Comparison of crater diameters to number of craters per square meter. Data collected from the LDEF intercostals and rows.

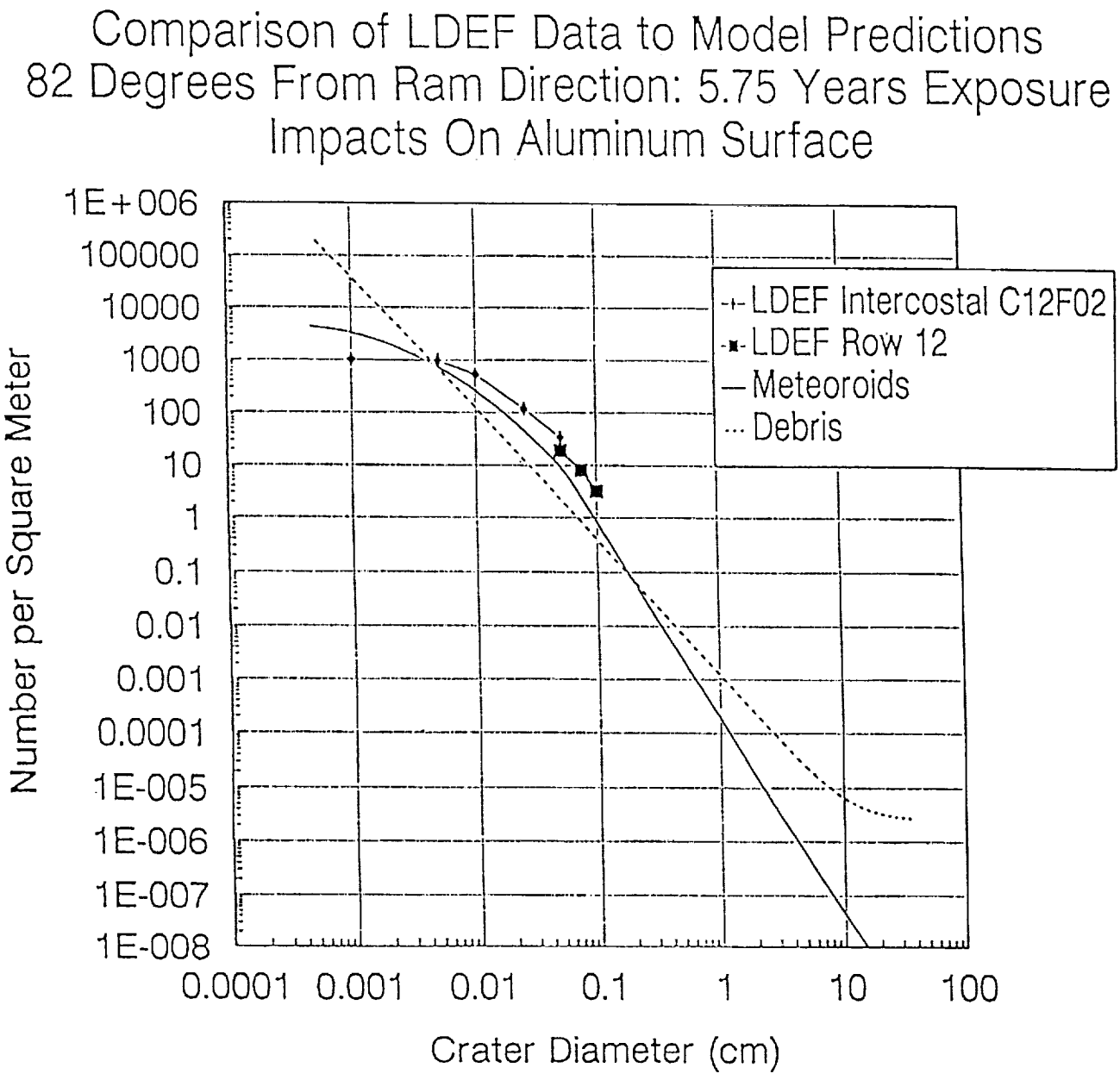

Figures 9j: Comparison of crater diameters to number of craters per square meter. Data collected from the LDEF intercostals and rows.

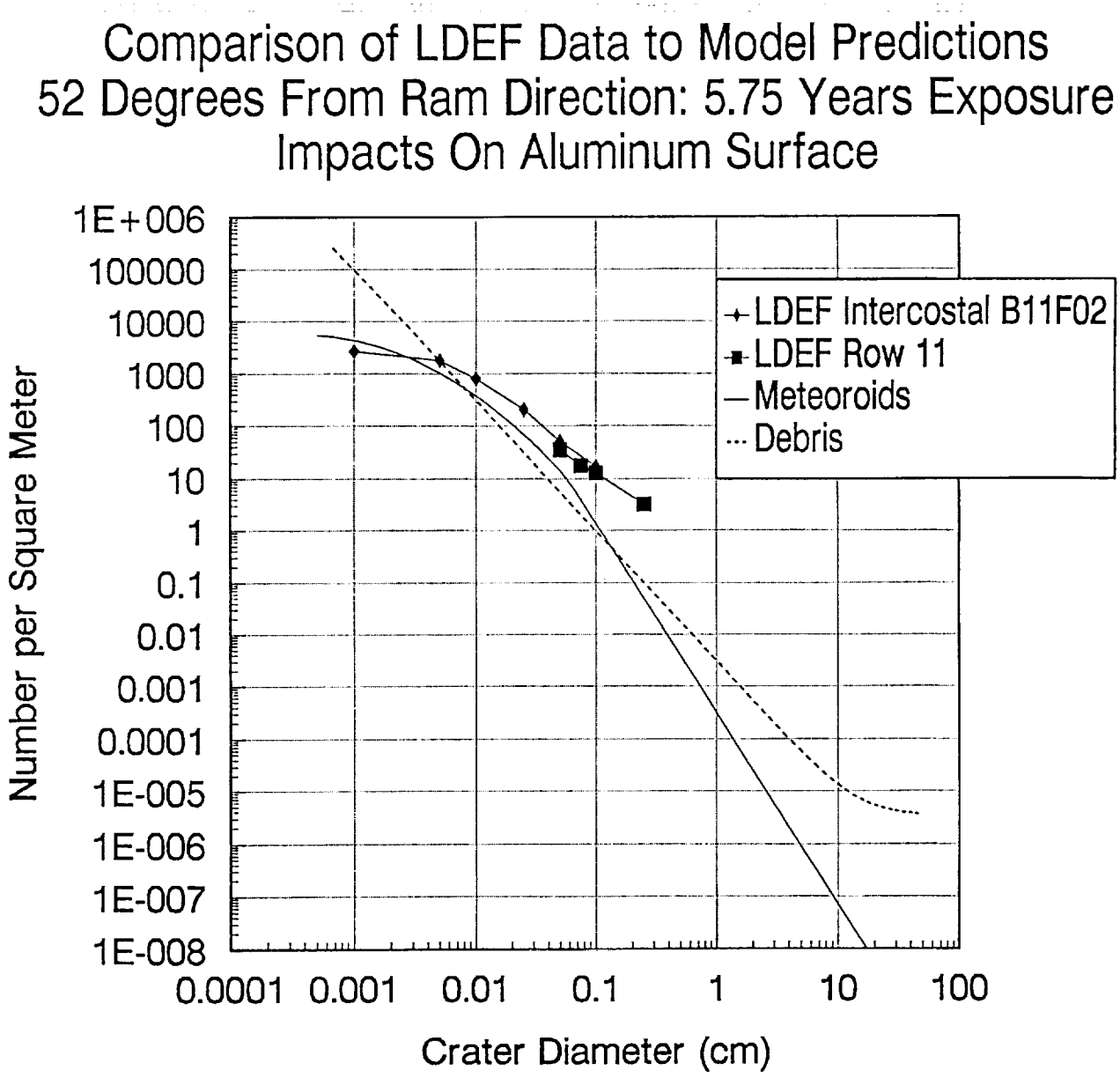

Figures 9k: Comparison of crater diameters to number of craters per square meter. Data collected from the LDEF intercostals and rows.

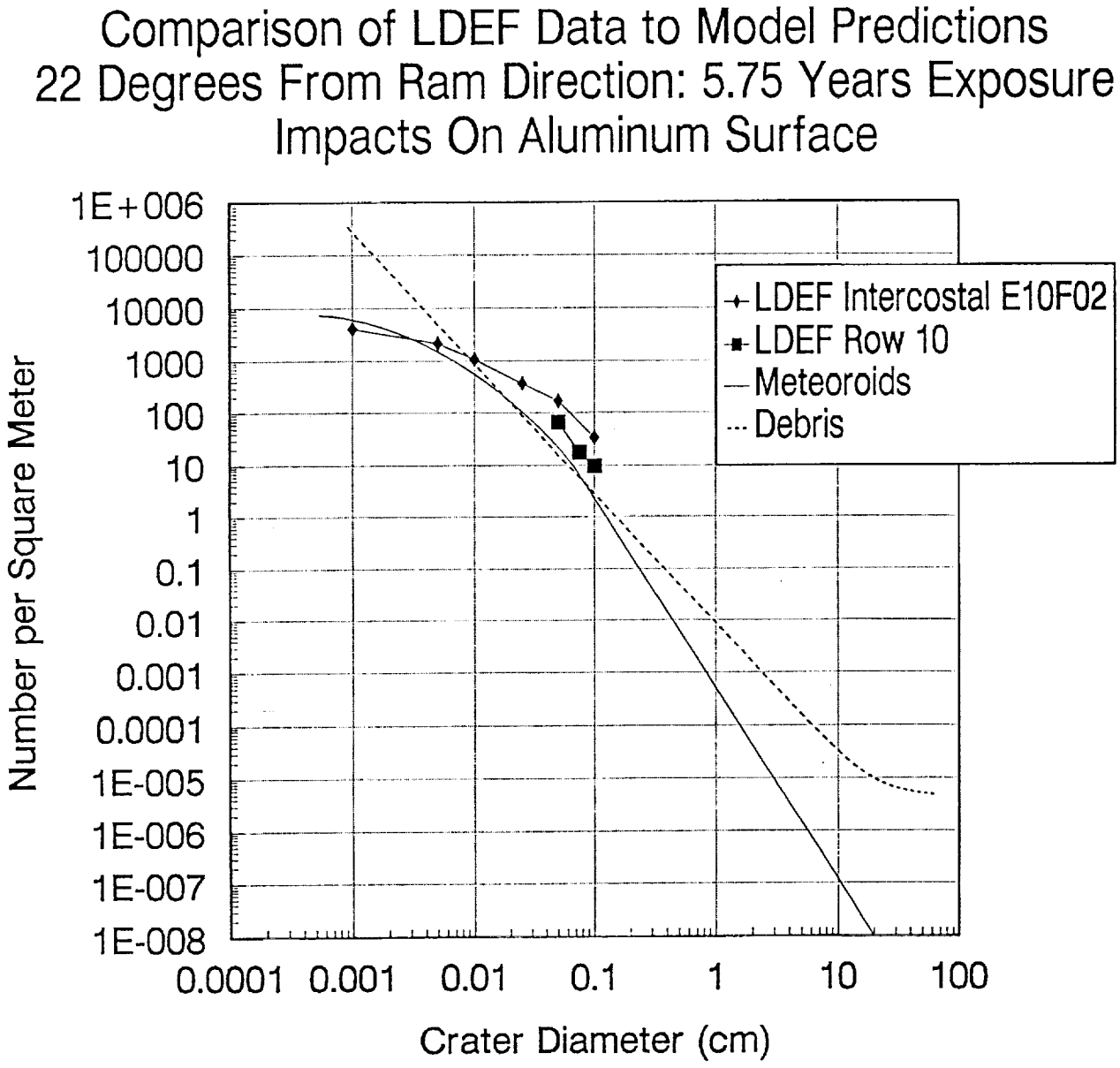

Figures 9l: Comparison of crater diameters to number of craters per square meter. Data collected from the LDEF intercostals and rows.

Overall, the measured data tends to oscillate around the predictions for the micrometeoroids. More specifically, the Kessler debris model[2] overpredicts the mean flux of small craters (~0.005 cm diameter), while the Cour-Palais micrometeoroid model[1] slightly underpredicts the mean flux for these small craters, for the RAM (row 9) surface. A similar divergence has been noted for the EARTH- and SPACE-facing ends (not covered in this report). This divergence may be indicative of either elliptical orbital particles from natural or man-made sources, of β-meteoroid fluxes, or a combination of the two. The Interplanetary Dust Experiment[16] data has positively identified a β-meteoroid component of the natural environment, which is not currently accounted for in the Cour-Palais model[1] we used. Grün *et al.*[17] did, however, take the β-meteoroids into account when they updated Cour-Palais' model in 1985. This version of the model is currently being analyzed and incorporated into our in-house SPENV model.

Other observed trends, most clearly seen in Figures 10a-e, include an asymmetry wherein the impact fluence tends to be greater than the predictions (for the crater sizes measured) towards the NORTH surface (angles in the range 0 to 180 degrees), and lower than predictions for the SOUTH surface (180 to 360 degrees, *i.e.* -180 to -0 degrees on Figures 8a-e). Scrutiny of Figures 9a-l also reveals a tendency for the data to exceed the predictions for the larger of the measured craters. Care must be exercised in the interpretation of Figures 10a-e. The "true" RAM direction is 0 degrees, and the micrometeoroid and debris models assume symmetry about this direction (the occasional "kinks" in these curves are due only to the interpolation routine in the graphing utility). If the environments were truly symmetric then the LDEF data would also be symmetric, regardless of the orientation of the rows and intercostals. The experimental data imply that the environment is **not** simply symmetric. We cannot explain this at present.

A caution should be raised with regard to measurements of the smallest craters: the target material is not pure aluminum alloy, but has an anodized surface (*i.e.*, an effective coating of alumina). For the larger craters this coating has negligible effect, but for the smallest craters the coating may constitute the "target". Since alumina has both a higher density and is tougher than

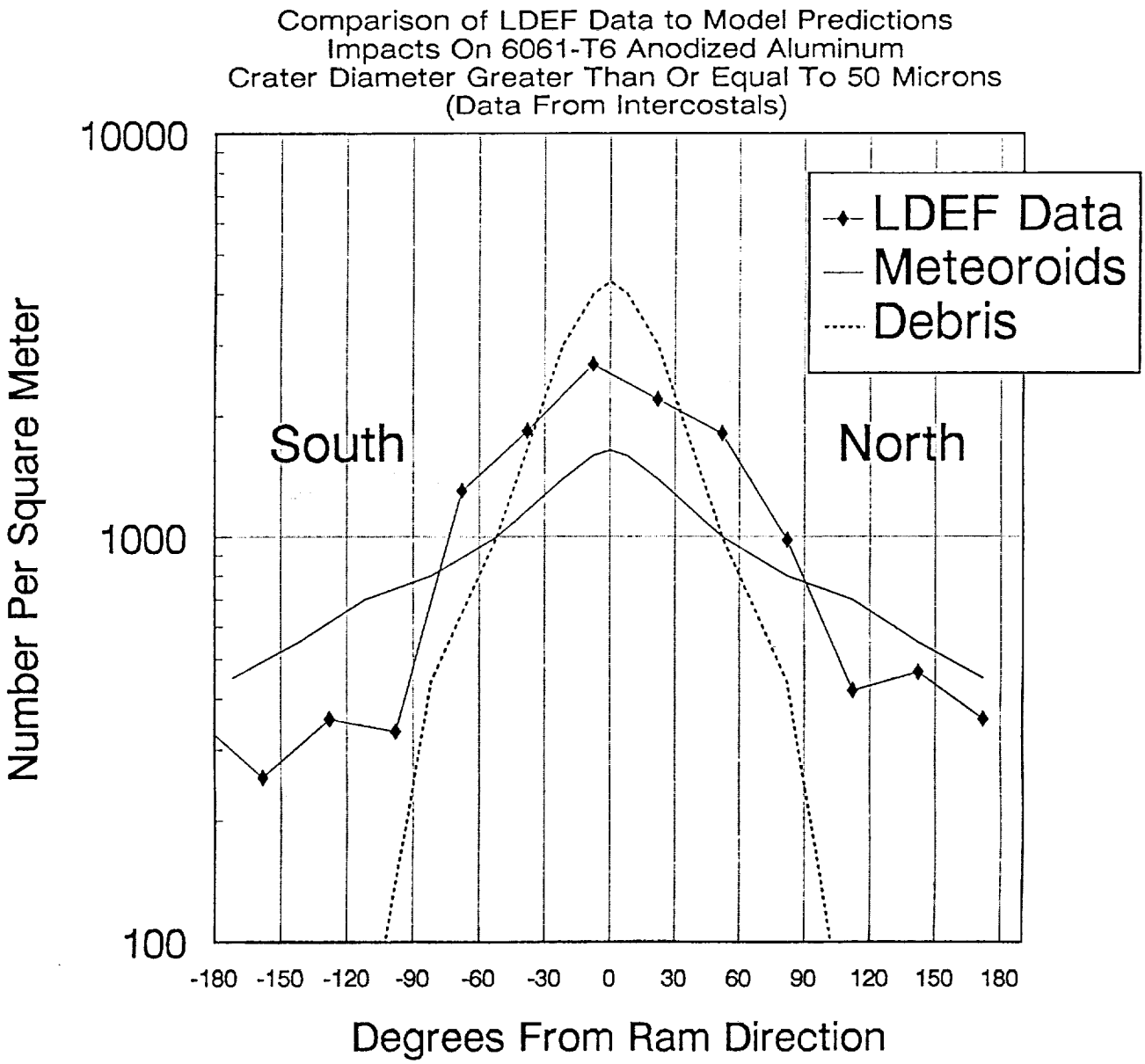

Figures 10a: Comparison between LDEF data and the M&D model predictions discussed in the text as a function of row location on the satellite.

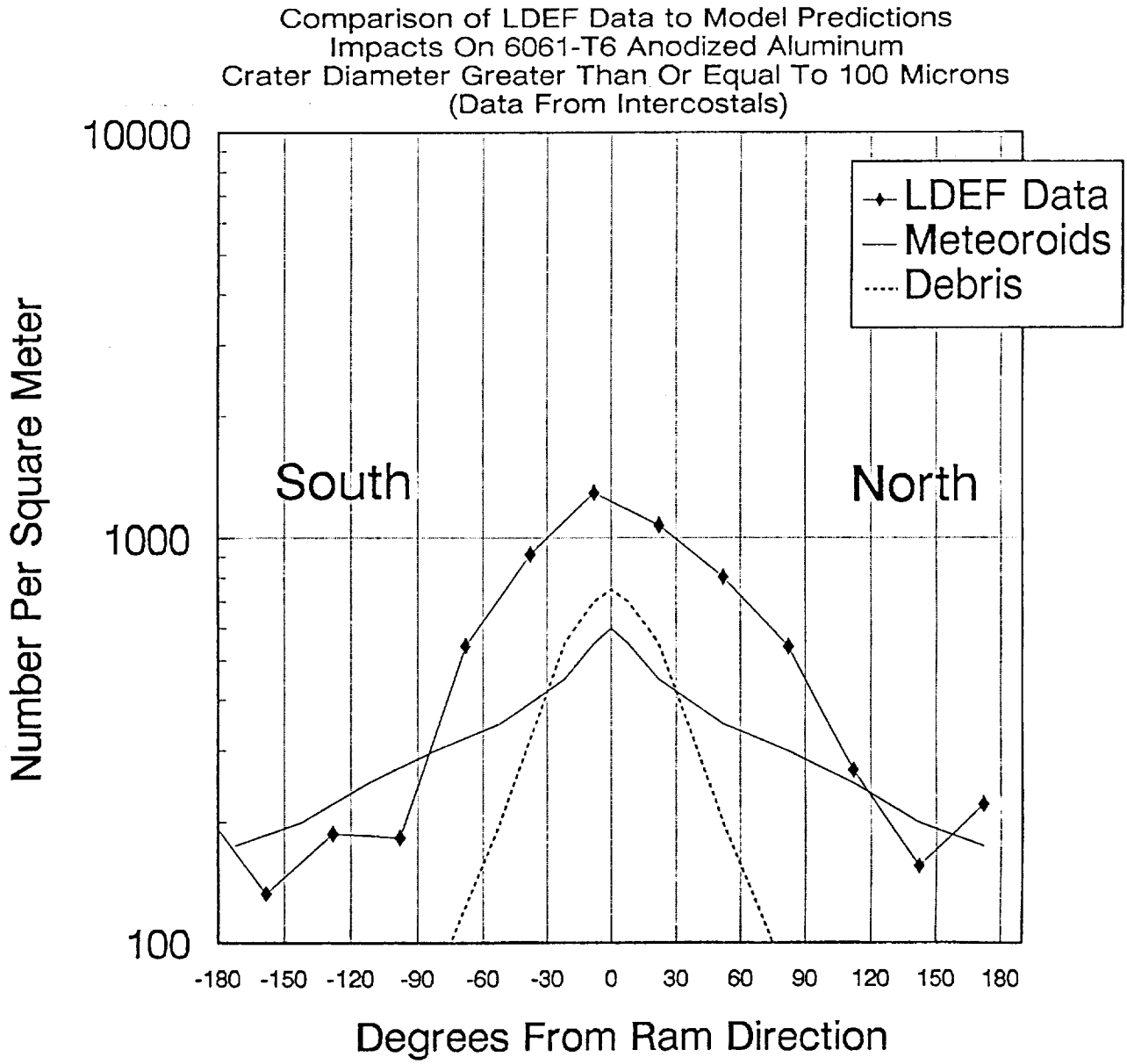

Figures 10b: Comparison between LDEF data and the M&D model predictions discussed in the text as a function of row location on the satellite.

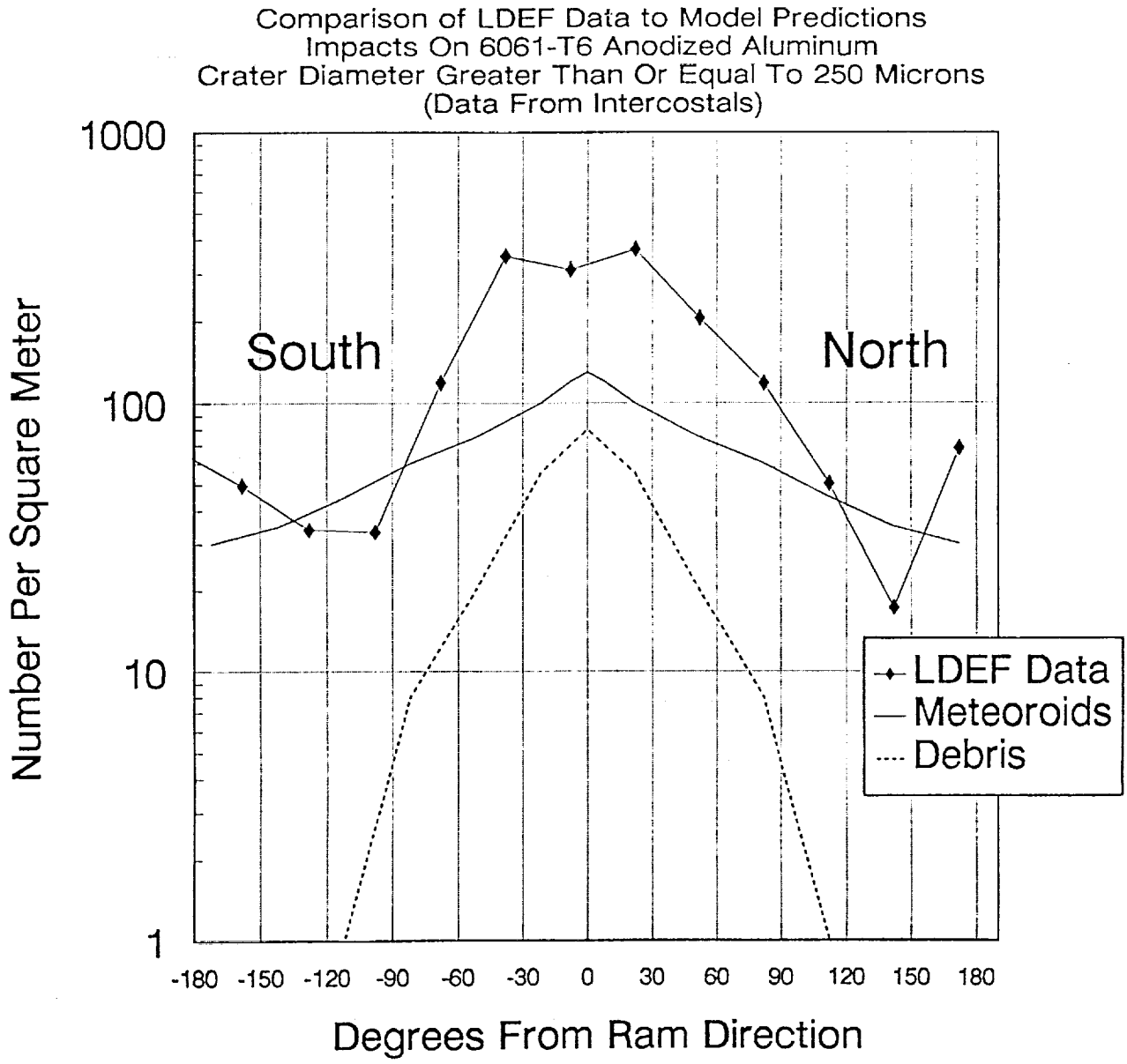

Figures 10c: Comparison between LDEF data and the M&D model predictions discussed in the text as a function of row location on the satellite.

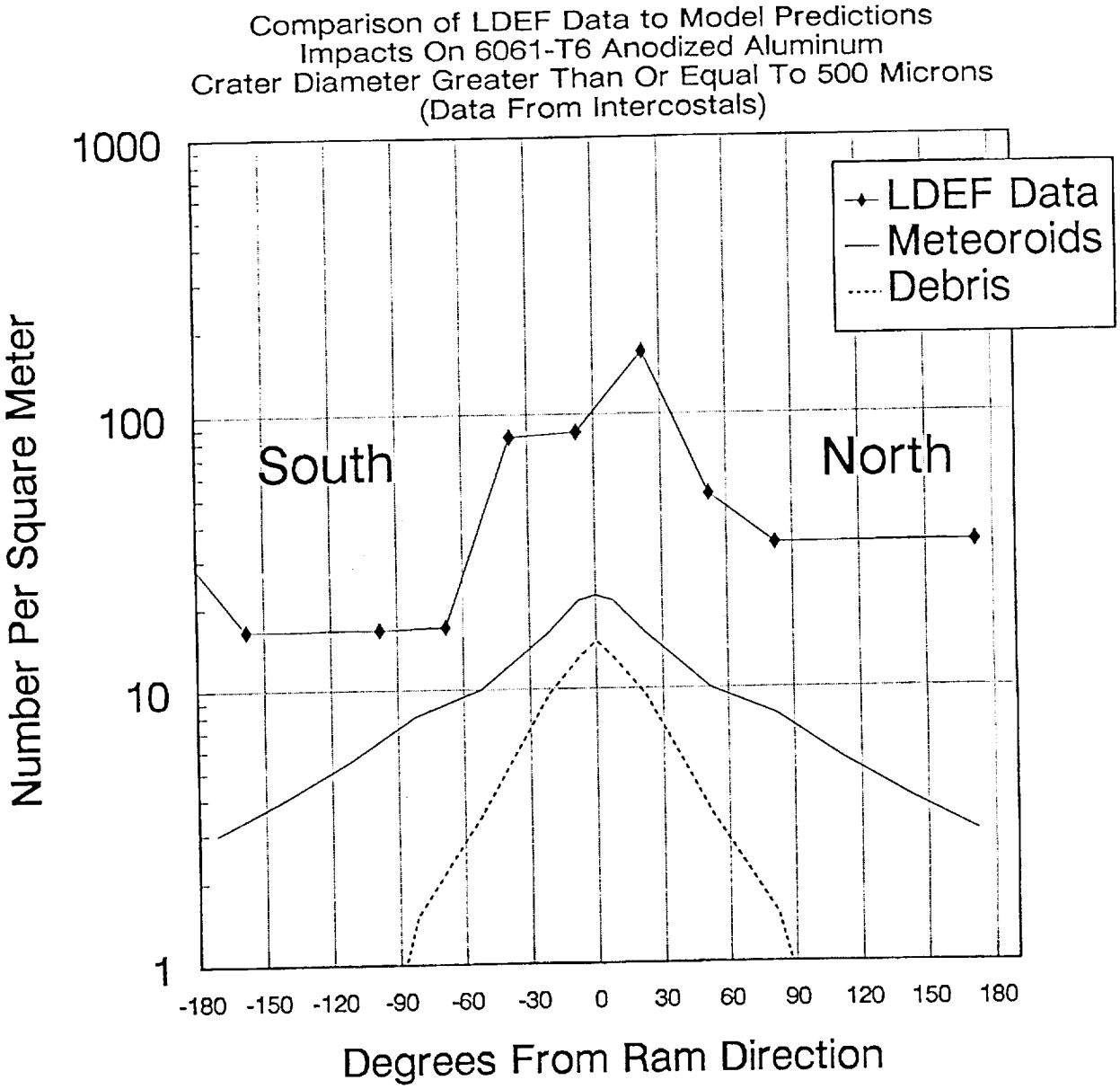

Figures 10d: Comparison between LDEF data and the M&D model predictions discussed in the text as a function of row location on the satellite.

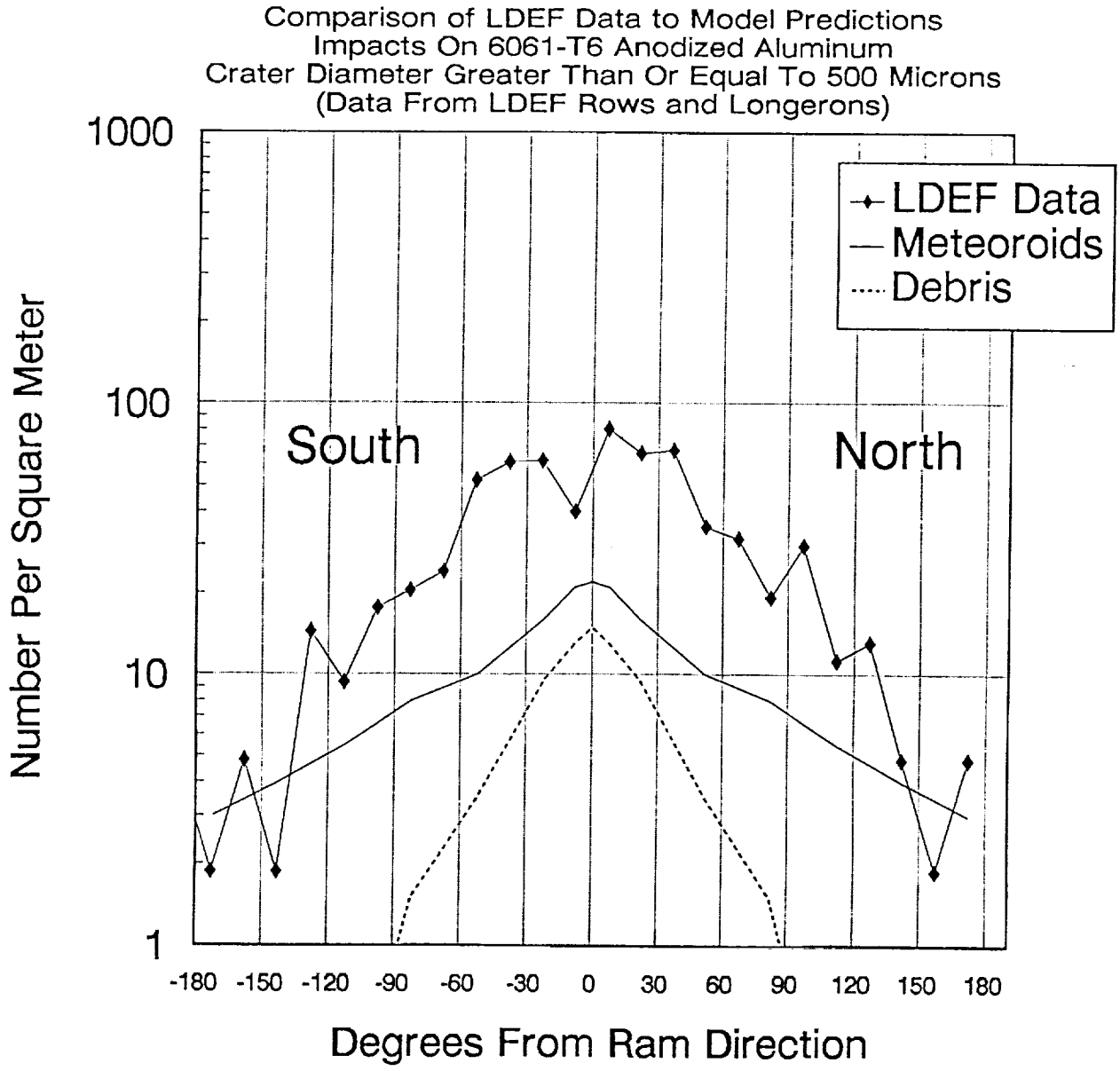

Figures 10e: Comparison between LDEF data and the M&D model predictions discussed in the text as a function of row location on the satellite.

Table 1: Statistical Information For LDEF Intercostal Data

Impacts On Aluminum Surfaces, Crater Diameters ≥ 10 μm

LDEF Row #	Degrees From Ram Direction	Intercostal Number	Surface Area Examined (m^2)	n = Number of Impacts Found	Impacts/m^2 (n/Area)	Error $\pm\sqrt{n}$	Scaled Error $\pm(\sqrt{n}/Area)$	Scaled Error %
1	112	B01F02	0.0594708	31	521.26	5.56	93.49	17.9%
2	142	B02F02	0.057873	41	708.45	6.4	110.59	15.6%
3	172	C03F02	0.0586895	30	511.16	5.48	93.37	18.3%
4	202	F04F02	0.0603608	18	298.21	4.24	70.25	23.6%
5	232	E05F02	0.0587443	97	1651.23	9.85	167.69	10.2%
6	262	B06F02	0.0600495	65	1082.43	8.06	134.22	12.4%
7	292	F07F02	0.058855	539	9158.1	23.22	394.56	4.3%
8	322	F08F02	0.0602198	172	2856.19	13.11	217.7	7.6%
9	352	F09F02	0.0579995	384	6620.69	19.6	337.93	5.1%
10	22	E10F02	0.059526	248	4166.25	15.75	264.62	6.4%
11	52	B11F02	0.0584148	158	2704.79	12.57	215.2	7.9%
12	82	C12F02	0.0590156	60	1016.67	7.75	129.71	12.8%

Table 2: Statistical Information For LDEF Row Data

Impacts On Aluminum Surfaces, Crater Diameters ≥ 500 μm

LDEF Row #	Degrees From Ram Direction	Surface Area Examined (m^2)	n = Number of Impacts Found	Impacts/m^2 (n/Area)	Error $\pm\sqrt{n}$	Scaled Error $\pm(\sqrt{n}/Area)$	Scaled Error %
1	112	0.6231	7	11.23	2.65	4.25	37.8%
2	142	0.6231	3	4.82	1.73	2.78	57.7%
3	172	0.6231	3	4.82	1.73	2.78	57.7%
4	202	0.6231	3	4.82	1.73	2.78	57.7%
5	232	0.6231	9	14.44	3	4.81	33.3%
6	262	0.6231	11	17.65	3.32	5.33	30.2%
7	292	0.6231	15	24.07	3.87	6.21	25.8%
8	322	0.6231	38	60.99	6.16	10.6	17.4%
9	352	0.6231	25	40.12	5	8.02	19.9%
10	22	0.6231	41	65.8	6.4	10.27	15.6%
11	52	0.6231	22	35.31	4.69	7.53	21.3%
12	82	0.6231	12	19.26	3.46	5.55	28.8%

the underlying aluminum, the result can be to reduce the crater sizes. This effect will produce a "skew" to the data, such that the plot of cumulative cratering artificially "flattens off" at the smaller sizes. Presently, we do not know the exact thickness of the anodized layer. However, we do know that if it is about 1 mil, then all craters below about 100 microns in diameter are affected.

Since impact events are assumed to be random it is appropriate to apply Poisson statistics to establish the appropriate standard deviations for the data. Thus, if the number of hits on a given area is N, the standard deviation is $+/- N^{0.5}$. Table I summarizes the data for the intercostals, giving the raw hit counts, the corresponding areas, and the resulting standard deviations, while Table II summarizes similar data for the rows. Since the investigated areas were usually considerably less than 1 square meter each, the error must be scaled up by the same ratio as the count rate in order to be consistent for quotes on a per meter squared basis. In Figures 9a-l there are overlapping data at some common crater sizes for the intercostals and the rows. Sometimes these data differ by more than a standard deviation of the **individual** data points. This more accurately indicates the true degree of uncertainty in the measured data. Such variations are to be expected, since Poisson statistics only apply for a truly random flux of impactors. As a simple example, if debris were really in circular orbits they would exist in striated orbits, since launches have not been made randomly into every possible altitude. It is the combination of (a) random collisional breakup, (b) air drag and, (c) initial elliptical launched orbits, that tend to give a randomization of the debris particles. Likewise, there is no *a priori* reason to believe that the micrometeoroids are truly randomly distributed. Data from the IDE[16] experiment on LDEF certainly indicate a degree of non-randomness *in time* showing apparent clustering behavior, and the integrated data from the F07F02 intercostal indicate similar effects with regard to *location.*

CONCLUSIONS

The comparisons provided herein demonstrate a good measure of the relative applicability of the environment models for first-order engineering design purposes, but illustrate the need for higher fidelity in the small impactor - spacecraft degradation - regime. One should be cautious in utilizing these comparisons to validate the micrometeoroid and debris models. The assumptions underlying these analyses are necessarily simplistic. For example, time-dependent variations associated with toroids or clouds of debris impactors (as inferred from the IDE experimental data) are not taken into consideration, nor is the fact that many of the debris impactors are in elliptical orbits around the Earth. The models and collected data do agree on several points however. Space debris does exist in all sizes, and has the possibility of growing into a potentially catastrophic problem, particularly since self-collisions between particles can rapidly escalate the numbers of small impactors. Kessler has deduced that a "runaway" escalation (which grows with the square of the population of particles) may already be occurring at an altitude of about 1000 km, where there is a local peak in the debris population.[2]

With regard to statistical errors, the data suggest that the true impact fluence, or flux, is rarely defined any better than one standard deviation (*s.d.*, Poisson logic) and is frequently only good to about three standard deviations, as evidenced by the "overlap" data taken on the intercostals versus the rows. Clearly, an updated model of the debris environment is required which incorporates elliptical orbits. Kessler[7] is presently addressing this issue, while an independent study is underway by Divine[18] at the Jet Propulsion Laboratory based on first-principles of orbital dynamics.

Updates in the scaling laws used to predict cratering are also needed. While this present study concentrated on the aluminum structure, there are many other target materials which suffered from cratering and/or perforations. Scaling laws are required to relate these various data. Presently, based on our own independent CTH computer modelling, we conclude that the

perforation limit equation of McDonnell[8,12] is credible, at least for symmetric impacts (*e.g.*, Al/Al). The McDonnell equation is cited **only** because it is one that we have been recently exercising. Other equations, such as those by Cour-Palais or Christiansen may be equally credible, we simply have not yet performed the necessary comparisons. However, more data and modelling are needed to establish generalized rules which account for both cratering and perforations for **any** combination of impactor/target and for wide ranges of impact speeds and angles of incidence.

Based on limited attempts to model impact events with the CTH code, we conclude that this hydrocode has the capability to realistically simulate many experimentally observed phenomena. A virtue of such a code is the ability to map out the sensitivities to assumed parameter changes, such as yield strengths, fracture strengths and interlayer bond strengths. Accordingly, we recommend further such computer studies in order to allow better understanding of impact events and correlations with experimental data.

REFERENCES

1. Cour-Palais B.G. *et. al.*: Meteoroid Environment Model - 1969 (Near Earth to Lunar Surface). *NASA SP-8013,* 1969.
2. Kessler D.J.; Reynolds R.C.; Anz-Meador P.D.: Orbital Debris Environment for Spacecraft Designed to Operate in Low Earth Orbit. *NASA TM-100471*, 1988. Also: D.J. Kessler, Orbital Debris Technical Interchange Meeting, Phillips Laboratory presentation, 2-3 April, 1991.
3. Bell R.L. *et al.*: *The CTH Code* (Version 1.024), Structural and Solid Mechanics Department, Sandia National Laboratory, Albuquerque, NM, October, 1991.
4. Atkinson D.A.; Watts A.; Crowell L.: *Final Report: Spacecraft Microparticle Impact Flux Definition.* Prepared for: LLNL, Univ. of Calif. by POD Associates, Inc., 1991.
5. Berhard R.P., See T.H., Horz F., Projectile Compositions and Modal Frequencies on the "Chemistry of Micrometeoroids" LDEF Experiment, Second LDEF Post-Retrieval Symposium, *NASA Conf. Pub.*, 1992.
6. Simon C.G. *et al.*: Elemental Analyses of Hypervelocity Micro-Particle Impact Sites on Interplanetary Dust Experiment Sensor Surfaces (abstract). Second LDEF Post-Retrieval Symposium, *NASA Conf. Pub. 10097,* 1992.
7. Kessler D.J.: Origin of LDEF Debris Impacts on LDEF's Trailing Surfaces. *Second LDEF Post-Retrieval Symposium*, 11 pp, NASA CP-3194, 1993.
8. Watts A.J.; Atkinson D.R.; Rieco S.F.: *LDEF Penetration Assessment: Final Report.* Prepared for Nichols Research Corporation, Dayton, OH by POD Associates, Inc., 1992.
9. Zook H.A.: Meteoroid Directionality on LDEF and Asteroidal Versus Cometary Surfaces (abstract). *In Lunar and Planet. Sci. Conf. XXII*, Lunar and Planetary Institute, Houston, TX, pp. 1385-1386, 1990.
10. Cour-Palais B.G., Hypervelocity Impacts in Metals, Glass and Composites, *Proceedings of the 1986 Symposium, Hypervelocity Impact,* Pergamon Press, 1986.

11. Christiansen E.L., Investigation of Hypervelocity Impact Damage to Space Station Truss Tubes, *International Journal of Impact Engineering, Proceedings of the 1989 Symposium*, Vol. 10, 1990, p. 125.
12. McDonnell J.A.M. *et al.*: An Empirical Penetration Equation for Thin Metallic Films Used in Capture Cell Techniques. *Nature, 309*, pp. 237-240, 1984. Updates with K. Sullivan, private communication, 1991.
13. Miriam Gersten: Maxwell Laboratory, Personal Communication, March 1992.
14. See T.H. et al.: Meteoroid and Debris Impact Features on the Long Duration Exposure Facility: A Preliminary Report. *NASA JSC #24608*, 1990.
15. See T.H. et al.: Detailed examination of LDEF's Frame and the A0178 Thermal Blankets by the Meteoroid and Debris Special Investigation Group (abstract). *Second LDEF Post-Retrieval Symposium*, 1992.
16. Mullholland J.D., and 8 co-authors (1991), IDE Spatio-Temporal Fluxes and High Time-Resolution Studies of Multi-Impact Events and Long-Lived Debris Clouds, *LDEF - 69 Months in Space, First Post-Retrieval Symposium, NASA CP-3134*, p. 517-528.
17. Grün E. *et al.*: Collision Balance of the Meteoritic Complex. *Icarus, 62*, 244-272, 1985.
18. Divine N. and Agüero R. C.: New Meteoroid Model Predictions for Directional Impacts On LDEF (abstract), Second LDEF Post-Retrieval Symposium, *NASA C.P. - 10097*, p. 56, 1992 .

Appendix

CTH Code Validation

APPENDIX

CTH CODE VALIDATION

The first task with the CTH code was to perform some type of validation between experimental results and reproducible computer simulations. The data and results from a series of gas gun experiments were provided by Dr. Fred Hörz of NASA Johnson Space Center.

The data provided by NASA contained many combinations of materials that were used for the impactor and the projectile. In order to get reasonably accurate results with the CTH code the materials chosen had to have material properties that were readily available and well characterized. Complex compound materials were ruled out, leading to a choice of an aluminum target and an impactor made of soda-lime glass. Results from the runs are illustrated below in Table A-1.

Table A-1: Data Comparison from CTH Run and Hörz et al. (1992)

Shot Number	Projectile Diameter (mm)	Aluminum Thickness (mm)	Velocity (km/sec)	Hole Diameter (mm) HÖRZ (1992)	Hole Diameter (mm) CTH
785	3.18	9.53	5.91	2.24	9.8
786	3.18	9.02	5.8	3.62	10
787	3.18	8.64	5.81	7.31	12.5
788	3.18	7.62	5.79	10.19	12.5
789	3.18	1.6	5.87	8.77	10
791	3.18	19.94	5.84	13.73*	11.000*

*These values are for crater diameters; they were not penetrations.

Several models were available in the CTH code, however, the one chosen was the Mie-Grüneisen. The variables used in the CTH runs are shown in Table A-2.

Table A-2: Variables used in CTH Calculations

Material	Density (g/cm^3)	Sound Speed (cm/sec)	Grüneisen	Heat Capacity ($erg/cm^3/eV$)	Constant in Linear Hugoniot
Aluminum	2.7	5.31×10^5	2.25	1.049×10^{11}	1.34
Soda-Lime	2.2	5.91×10^5	0.4	8.744×10^{10}	1.5

The aluminum alloy that was used in the experiments was Al-1100 variety, but the temper was not known. The temper of the metal can result in large changes in the tensile strength and the yield strength. In order to match the experimental results, it was necessary to run several calculations that used a range of yield and tensile strengths. The final values that were arrived at are listed in Table A-3:

Table A-3: Yield and Tensile Strengths Used in CTH Calculations

Material	Yield Strength (kbar)	Poisson Ratio	Fracture Stress (kbar)
Aluminum	1.3	0.35	1.6
Soda-Lime Glass	10	0.16	1.2

The primary goal of this series of runs was to replicate the wall penetration limit that was seen in the experimental results. The final values listed above successfully simulated this experimental limit. Exact replication of the hole diameters for penetration was not expected, since only small changes in velocity or material properties produce rapid changes in the perforation. The aluminum alloy that best matched the NASA-JSC data was identified as Al-1100-H16. The data chosen for the soda-lime glass were based on quotes from manufacturers and reference data for various glasses. The CTH calculations indicated only a moderate sensitivity to parameter changes for the glass impactor, but large sensitivity to the

values for the aluminum target. No attempt has yet been made to model other experimental data, such as that for the Al foils used by McDonnell.